SIDE EFFECTS OF THE UKRAINE INVASION: THE ENVIRONMENTAL INFLUENCE OF THE BYPASS OF UKRAINE & RUSSIA ON GLOBAL AVIATION UTILIZING THE BOEING 777 FLEET

E. Schuster*, M. Uijt de Haag*
* Technical University of Berlin, Chair of Flight Guidance & Air Transport, Marchstraße 12-14, 10587 Berlin, Germany

Abstract

Undoubtedly, the flight of a complex aircraft between two locations is associated with a significant engine fuel consumption leading to a likewise significant as well as complex environmental burden. With improved understanding of the environmental impact of flights from extensive research, the present work utilises a validated model for the main engine's fuel consumption applicable to Boeing 777's using the GE90-110 engine base.
Methodologically, the engine fuel consumption model used in this paper incorporates EUROCONTROL's widely accepted BEAM model, which is overarched by, e.g., an incorporated complex weather model. It uses a MERRA-2 product harmonised with METAR information per flight trajectory-relevant airport. This information as well as information from other submodels is passed into an emission evaluation model that relies on Boeing's Fuel Flow Method 2.
Applying the approaches, the authors examine the corresponding emission substances for the provided flight trajectories over an eight month period starting at the beginning of the year of the Ukrainian-Russian conflict, 2022. For a more detailed knowledge and understanding, the findings are compared with the corresponding reference period in 2019 (as pre-Covid-19 basis). Although fairly low resolved, the trajectories for the respective time intervals were aggregated through Flightradar24, which utilises a filtered combination of position determination through ADS-B, radar, and multilateration information. The rationale for using this data is based on the relatively easy access of the data compared to actual Flight Data Recorder reports.
In total, for both years 276,536 original flight events of different quality are provided, which implies the need for flight event recombination if the flight event is of a cross-day character. Thus, the day-wise recombination for the individual year 2019 and 2022 left 97,083 and 131,952 for further evaluation.
Additionally, not all the supplied Flightradar24 data can be used in above-mentioned models due to data integrity problems. Therefore, the provided trajectories are screened for three error types: (A) a range check, (B) a data gap check, and (C) trajectory completeness. After recombination and data cleaning,
The aggregated results show a significant increase in aircraft movements in the year 2022 by 37.04% that lead to well above 9.5mio.t of carbon dioxide emitted. Thus, a significant contribution to increase the aviation-imposed environmental burden is ascertained. Therefore, a multilayered flight event deduction was performed to identify the trajectories that penetrate the focal airspaces of Ukraine and Russia. These analyses have determined the influence of the flight numbers, routes, and individual operators. Subsequently, the more and less restriction-affected operators have been identified. An airline from Far East Asia experiences the most striking year-to-year changes introduced by the airspace bans resulting in a notable emission of primary and secondary constituents. Finally, the prominent effort-added for German B777 operators has been quantified.

Keywords

Environmental Burden; Trajectory Analysis; Engine Fuel Consumption; Ukrainian-Russian Conflict

doi: 10.25967/610082

NOMENCLATURE

Roman Symbols

FC	Fuel Consumption, kg
f	BADA BEAM fuel coefficient, diff. units
FF	Fuel Flow, $\mathrm{kg\,s^{-1}}$
n	Number, km
OC	Oil Consumption, $\mathrm{qt\,h^{-1}}$
R	Range, km
t	BADA BEAM thrust coefficient, diff. units
Thr	Thrust, N
T	Temperature, $\mathrm{m\,s^{-1}}$
t	Time, s
v	Speed, $\mathrm{m\,s^{-1}}$

Greek Symbols

Δ	Difference operator
μ	Arithmetic mean
σ	Standard deviation

Subscripts

adj	Adjusted
Block	Block
CRZ	Cruise phase
dev	Deviation
DP	Data Point
FE	Flight Event
max	Maximum
min	Minimum
Ref	Reference
Reg	Regression-based
TAS	True Airspeed
x	Coefficient counter

Acronyms / Abbreviations

AAW	Actual Aircraft Weight
ADS-B	Automatic Dependent Surveillance - Broadcast
B777	Boeing 777
BADA	Base of Aircraft Data
BEAM	BADA Enhanced Approach to Modelling
CFR	Code of Federal Regulations
CSV	Comma-separated values
DFS	Deutsche Flugsicherung
DP	Data Point
FAA	Federal Aviation Administration
FDR	Flight Data Recorder
FE	Flight Event
FIR	Flight Information Regions
FLARM	FLight alARM
FN	Flight Number
FOB	Fuel on Board
FR24	Flight Radar 24
GES DISC	Goddard Earth Sciences Data and Information Services Center
GPS	Global Positioning System
IATA	International Air Transport Association
ICAO	International Civil Aviation Organization
ID	Identification Number
IQR	Interquartile Range
ISA	International STandard Atmosphere
LH	Long-haul
MERRA-2	The Modern-Era Retrospective analysis for Research and Applications, version 2
METAR	Meteorological Aerodrome Reports
MH	Medium-haul
MTW	Maximum Taxi Weight
NASA	National Aeronautics and Space Administration
NOTAM	Notice to Airmen/Notice to Air Missions
OBW	Off-block Weight
OC	Oil Consumption
OEW	Operating Empty Weight
OL	Oil Level
PDF	Probability Density Function
PIA	Pakistan International Airlines
PL	Payload
SH	Short-haul
UAE	United Arab Emirates
UIR	Upper Flight Information Region
Y2Y	Year-to-Year

1. INTRODUCTION

Without a doubt, aviation has a non-negligible impact in altering local and global air composition. Hence, this transport mode is widely accepted to be classified as having a negative impact on both local air quality and climate change. In the last decade, there has been an increase in the amount of effort in modelling aircraft operating-induced emission in the scientific community. Especially, in the following fields:

- fuel consumption (FC) modeling of a generic (e.g., [1], [2], [3], [4], [5], [6], [7], to name a few) and individual nature (e.g., [8], [9]),
- emission and dispersion modeling with their atmospheric coupling characteristics, and side effect coupling (i.e., [10], [8], [11], [12], [13], [14], [15], [16], [17], and [18] to name a few) etc.

Research in these fields has been highlighted as relevant under the increasing societal awareness for this transport sector's emission responsibility. In fact, this focus is almost exclusively based on the thrust engine-related fuel burn, with minor digressions into the Auxiliary Power Unit-related fuel burn. Generally speaking, other air-altering constituents must be considered under-represented in the scientific community. This context can be, e.g., traced back to issues with proprietary data and data privacy entitlement, and, subsequent challenges in receiving detailed, structured information by the respective participants in global aviation.

The development of these models, undoubtedly, has created the baseline for a common understanding in aircraft operation and its consequences for the environment and mankind.

In the present work, this context is identified and the role and influence of the *B77L*[1] (aircraft-individual as-

[1]This International Civil Aviation Organization (ICAO) aircraft descriptor likewise contains the aircraft types of Boeing 777-200LR (passenger version) and 777-F (freighter version).

sessment similar to [19]) will be evaluated and challenged after a general introduction to the historical background.

1.1. The Invasion of Ukraine

In February 2023, the century-long political tensions between Ukraine and Russia increased as a consequence of the latest aggressive Russian campaigns of the annexation of the Crimean peninsula (2014) and the political recognition of the proclaimed (but internationally unrecognised) separatist territories of Luhansk and Donezk on 21st February 2021. Both agitations paved the way to the 24th February 2022 when the strained relationship culminated in the Russian invasion of the Ukrainian territory. In addition to the humanitarian or economical drawbacks, the attack imposed massive repercussions on the respective national and international aviation, which will be focused in the present work. Currently, the Deutsche Flugsicherung (DFS) has set a *Level 3* risk level prohibiting civil German air operators to penetrate the Flight Information Regions (FIR) of Dnipropetrovsk, Simferopol, Lviv, Odesa, and Kyiv as well the latter's Upper Flight Information Region (UIR). Beginning the 25th February 2022, parts of the Russian and the Belarusian airspace (FIR Moscow, Rostov-Na Donu, and Minsk) are being considered a *Level 2* risk with possible usage of weapons against operators and are, thus, recommended to be avoided, the DFS announced [20]. The Federal Aviation Administration (FAA) agrees with their published Notice to Airmen/Notice to Air Missions (NOTAM/NOTAMs) issued in [21] and [22], respectively.
The developed international tension has introduced a wave of airspace bans initiated by the government of the United Kingdom towards the Russian air operators. As a respective adversarial action, Russia announced the same for British aircraft on the following day. Up until 1st March 2022, the two conventionally formed opposite systems, namely the Western countries (e.g., European Union, Canada, and USA) and Russia have mutually banned each other's operations in their relevant airspaces [23–25]. As a direct consequence, international aviation as a whole has faced a strict increase in economic and financial expenses. Here, e.g., [24] highlights the increased flight time and the incorporated additional fuel burn[2] (plus imminent additional refuelling stops if needed) for Western operators relying on Russian airspace. The context is exemplified in Fig. 1 that clearly shows the trajectory rerouting due to the Russian airspace ban. For example, on 7th March 2022 Air France flight number AF276 (Paris to Tokyo) used a southern route avoiding Ukrainian and Russian airspace as well as the Simferopol FIR (controlling the airspace around the Crimean peninsula) with the airspace ban effective. In contrast, the JL44 flight from London to Tokyo performed a route via the North Atlantic, North Pacific to its destination. It is noteworthy that the scientific community agrees to evaluate LH FE with a South East Asia direction originating from Finland (mainly by Finnair) as an operational worst-case scenario (in terms of routing, incorporated fuel burn, and additional flight time) [23, 24, 26, 28]. Furthermore, the relation is also applicable to Russian airlines operating nationally to/through the Kaliningrad FIR and internationally conceivably close to or through foreign airspaces.

FIG 1. Exemplary visualization of flight AF276 using B77W prior and after Russian airspace ban. Flight JL44 performed a similar route as AF276 on 26th February 2022 with significant re-routing adjustment from 7th March 2022. [29]

The references [30] (as freighter operation is highly reliant on routes from Europe to Asia) and [27] elude or directly refer to the additional costs with regard to the transport of goods or the aircraft maintenance. Whereas the former issue concerns both side's operators, the latter is significantly more stringent for Russian operators as, e.g., the acquisition of replacement components for the aircraft manufactured by Airbus or Boeing is prohibited by the respective Western countries leaving Russian operators almost exclusively with black market or other (in the understanding of Western countries) illegal replacement acquisition options. In addition to various other repercussions, the authors want to highlight the dependency of Western aviation manufacturers and their suppliers on Russian titanium that leads to increased costs as new/different sources and/or supply chains must be established [26,31]. Further influences can be deduced from [32]. For purposes here, the authors have decided to omit indirect effects such as the influence of the crisis on neighbouring countries as part of a spillover effect as substantiated by [25].
In any case globally, Russia is left isolated from western markets by bans, sanctions, and embargoes from the western pole that instate nonnegotiable fronts. As a consequence of the country's dimensions the dependency on Asian markets, Western operators face added efforts when offering preinvasion established routes. This relation describes the rationale for increasing re-

[2] That includes the crisis-incorporated oil, and thus kerosene, prices. [24, 26, 27]

search effort with respect to the environmental impact of mutually significant airspace bans on various civil air operators.

2. METHODOLOGY

In this chapter, the reader is introduced to the applied models for the calculation emissions as appeared before in [9]. Both model descriptions are presented as an overview to introduce the reader to the created approaches.
Generally, the reader should note that the modelling approach presented relies on a series of assumptions. Here, the authors emphasise that the model is created and validated from FEs performed with a B777-200LR/B777F. Subsequently, separation of aircraft type cannot be allowed. That also incorporates the fact that the type of aircraft used is equipped with GE90-110B1 engines. Here, the authors neglected the engine's maintenance and modification status (that can be identified as influence, e.g., to the engine oil consumption) as well as differences with regard to the engine's subtype ("-110B1"). Subsequently, it is assumed that all FEs were performed with this explicit engine type. Furthermore, the aircraft-engine integration is also not explicitly reflected by the model which could lead to additional FC. The system/component status is indirectly presented by the content of the FDR report snippets only, but not specifically evaluated.

2.1. Data Aggregation & Handling of FR24

As the work aims to improve the understanding of emissions to the public, the authors also tested the performance of the incorporated models against, among others, the ADS-B data of the respective flights, gathered from the provided FR24 data sets[3]. Furthermore, FR24 utilises multiple information to deduce a specific aircraft position (state), which requires filtering to reduce the respective and combined measurement uncertainty. Even though receivable (as ADS-B transponder-equipped aircraft transmit the data continuously) with fairly low-cost equipment, ADS-B data are prone to various issues like eavesdropping of the relatively nonsecure communication, jamming, or message injection/modification, reports [37]. Furthermore, there are various aircraft not equipped with the technology, namely smaller or older aircraft[4]. Therefore, additional data aggregation approaches are followed. Briefly, the FR24 data originate from ADS-B (ground and satellite-based), multilateration, and radar data [38]. In the present work, the relevance of portable collision avoidance system sources such as FLight alARM (FLARM) or the Open Glider Network are neglected.

[3]The regulatory technical background on ADS-B is extensively explained in [33], [34], [35]. Interpretation of ADS-B can be found, among others, in [36] or [37]

[4]Not to be generalised as the technology can be (and under circumstances should) be retro-fitted (cf. Code of Federal Regulations 14 CFR 91.225 and 14 CFR 91.227)

The server-based original data was provided by FR24. To ensure the readiness of the data provided, the authors established a data handling process that is visualised in Fig. 2. The handling input data is composed of the individual flight events containing rudimentary information of

- the aircraft's 4-D position (with Zulu timestamp and UNIX timestamp),
- the flight number, altitude[5],
- ground speed, and
- flight direction.

In addition, a daily flight summary is offered. It is composed of

- a flight identification number (ID)[6],
- an aircraft ID,
- the aircraft's registration,
- the aircraft type,
- the callsign,
- the flight number,
- scheduled origin airport,
- scheduled destination airport, and
- actual destination airport.

As the files are separated per day, they have been recombined to complete the respective trajectory and create the target Comma-separated values (CSV). Furthermore, the trajectories are passed through a gate keeper to ensure data consistency (data gaps greater than 3 h return a file rejection and, thus, lead to the termination of the process). The accepted files will be offered to the proposed model introduced in Sec. 2.2.

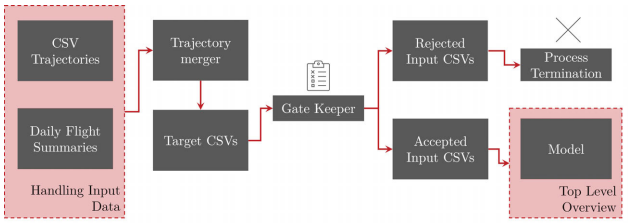

FIG 2. Data handling procedure for the aggregation of FR24 CSV input files (own figure).

After recombination and cleaning, the data input contains 57.60% of the year 2019 data are rejected leaving 57,183 files open to be used for the calculations. For the year 2022 44.69% of the 141,673 flight events are rejected using the above criteria, introducing a notable reduction in files.
This results in the evaluation of 739,280,407.68 km travelled in 135,549 flights performed by 291 unique aircraft connecting 443 unique airports across both years. The authors assume the defined setup as representative of the actual fleet movement with relevance to the northern or southern bypass of Russia.

[5]Notably, FR24's understanding of *altitude* does not comply with the technical term that references to the QNH alone.

[6]The authors assume that to be a company-internal numbering logic.

2.2. Top Level Design

The present model is created from FDR reports[7] that are assumed to be the *single-source-of-truth*. Subsequently, the created submodels were validated against the FDR data. To offer an open source approach to the usage of the submodels, the authors decided to evaluate the submodel performances against data reports provided by Flightradar24 (FR24) (see Sec. 2.1 to get an overview of the aggregation and structure of FR24 data). Thus, with the gathered observations from the respective model validations, an appraisal of the broad application of FR24 data as input data can be manifested.

To better illustrate the modelling approach, see Fig. 3. The top-level model process is initiated with the preparation of the input data. Thus, the provided trajectory will be aligned with the upfront defined calculation requirements (e.g., numerical inputs (weights, oil level), state inputs (e.g., METAR, interpolation functions, calculation frame), and other supplementary calculation properties). Subsequently, a gate keeper analyses the flight trajectory for two additional requirements that lead to FE rejection if not met:

- A disagreement of calculated great circle distance[8] per DP and in summation the aircraft's maximum range, and
- an incompleteness of the trajectory (minimum missing one of the airport of origin and destination).

In case of a positive rating, the calculation will proceed to the calculation of the main engine consumption. This portion consists of multiple supplemental models. Foremost, the FC calculation is based on the BADA BEAM approach defined in [1]. Furthermore, a weather module is arranged together with additional cooperative submodules and is supported with the use of databases of, e.g., aircraft, airports, and regression parameters.

The reader should note that the emission assessment can solely be performed as a result of the FC calculation. Moreover, the *Emission Evaluation* that allows the calculation of the primary and secondary emission residues applies the Boeing Fuel Flow Model 2.

2.3. Main Engine Fuel Consumption & Emission Evaluation

To aggregate the aircraft emissions across the provided trajectories, a model developed by the authors [9] is used that is designed to be applicable to the relevant aircraft type. The model is based on the BEAM model (see [1] for further information) to calculate the FC of an individual flight event using B77L. In BEAM, various coefficients for the calculation of thrust tc_x and fuel flow fc_x are introduced through said reference. As per Eq. 3.1-10 of [1] the thrust is calculated as follows:

$$Thr = tc_7 \cdot (tc_0 - tc_1 h + tc_2 \frac{1}{v_{TAS}} - tc_3 \frac{h}{v_{TAS}} + tc_4 h^2) \cdot (tc_6 - tc_5 \Delta T_{ISA}). \quad (1)$$

Consequently, the fuel flow FF is gathered through:

$$FF = fc_5 \cdot (fc_0 - fc_1 h + (fc_2 + fc_3 v_{TAS} - fc_4 v_{TAS}^2) \cdot Thr)). \quad (2)$$

The developed approach introduces a non-ISA model using MERRA-2 data in combination with official METAR data representing the local atmosphere in airport-near air parcels. Additionally, a temperature-dependent correlation was detected and its influence is compensated by an implemented correction factor to the respective thrust calculation. Consequently, the model was validated against FDR data of a B77L operator. Further comparative validation was performed using FR24 data, which, ultimately, allows the provided data to be applied as input data set to the authors' model [9].

Fig. 4 illustrates the model performance against the FDR data and further details the model performance when clustering the FR24 input data set into SH, MH, and LH flights. For the sake of understanding, a time-dependent clustering requirement is used. For this reason, flight durations up to 180 min are considered a SH FE. The time interval between 180 min and 360 min determine an MH FE, and consequently a flight time greater than the last requirement defines a LH flight. Obviously, the model shows its weakspot in the SH portion. Across all FE types, the model performance is considered acceptable as the median achieves – 1.13 t with a standard deviation σ of 2.89 t ($\triangleq$ – 3.93 $\pm$ 11.98%) compared to the proposed model with FDR sets.

In contrast to the procedure described in [9], the model input with respect to the present paper's focus has been further adjusted as detailed individual FDR reports (including actual aircraft weight information per timestamp) are not available for the relevant time period. Adjustments include, i.e., the aggregation of weather data (here: MERRA-2 and METAR information), as well as weight inputs. The former will be collected through publicly available data[9], the latter will be separated into three subclusters with maximum and minimum off-block mass, and a common trajectory-individual off-block weight (OBW) deduced from FDR data of [9]. This approach yields the following equations that are a result of the limited availability of data

[7] Henceforth, the term *FDR report* and *FDR extract* is used interchangeably.

[8] A range check failure references to a GPS position error, where the timestamp is not corrupted. The inter-DP great circle distance was calculated using the Haversine equation.

[9] Data is provided through NASA GES DISC data and the IOWA Environmental Mesonet Network.

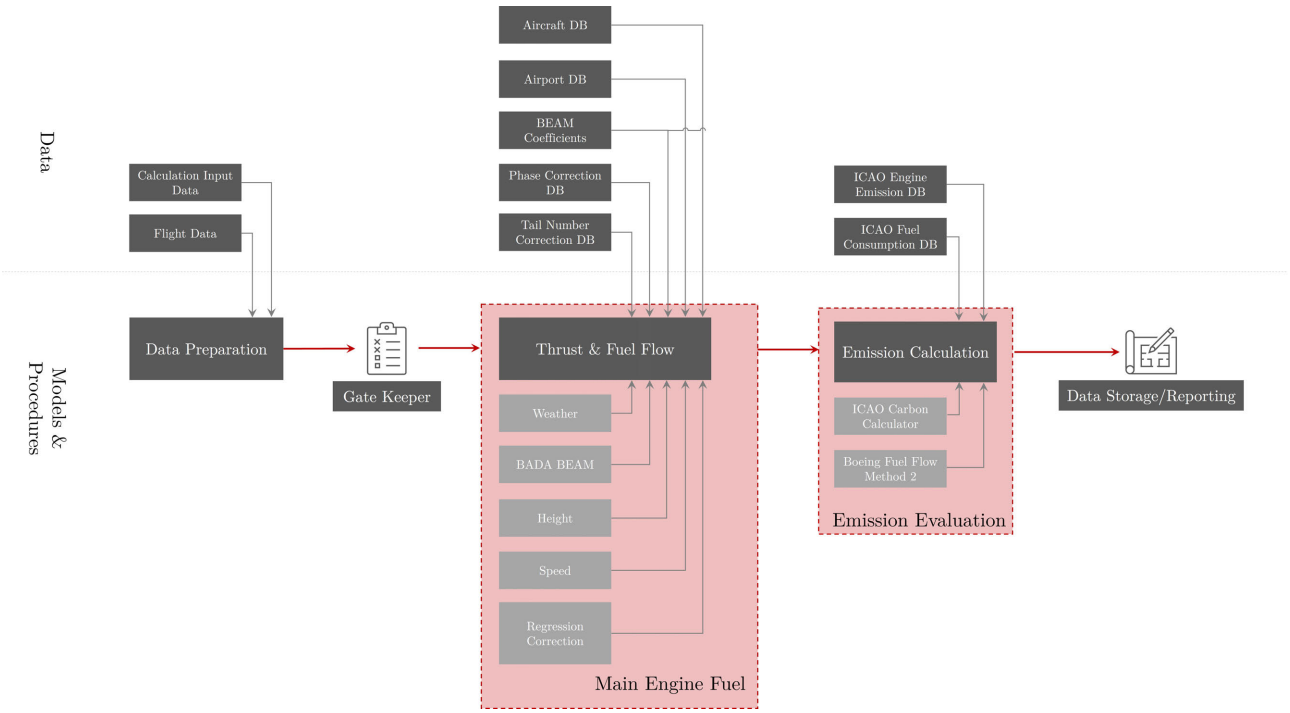

FIG 3. Top level overview of the modelling approach (own figure).

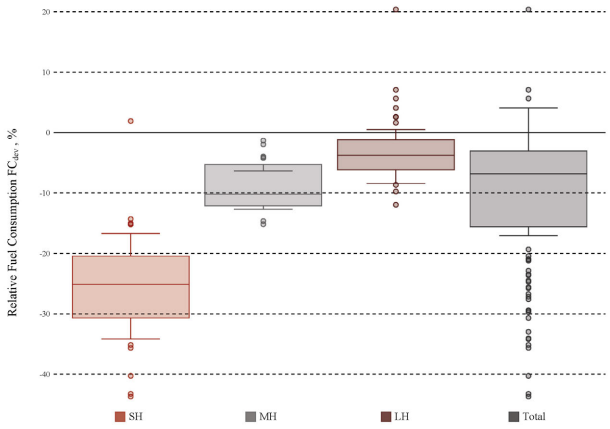

FIG 4. Relative Performance of the proposed model from [9] against FDR data when applying FR24 data (own figure).

and the sequential nature of the code.

(3) $OBW_{min}(R) = OEW + FOB_{Reg}(R)$ and

$$OBW_{max}(R) = OBW_{min}(R) + PL_{max}$$

The minimum OBW weight determination is the result of the aircraft structural Operating Empty Weight (OEW) and the regression-based Fuel on board (FOB) to commence the respective route. According to Eq. 3, OBW_{max} is allocated from the range-dependent OBW_{min} with the maximum payload PL_{max}. The developed weight corridor (between the grey and orange distributions) with the identified regression-based weight from [9] is presented in Fig. 5 as shown in the following illustration. The relevant frame of consideration for the B77L is presented in light grey. It is determined through the maximum range R_{max} and the OEW and Maximum Taxi Weight (MTW) respectively.

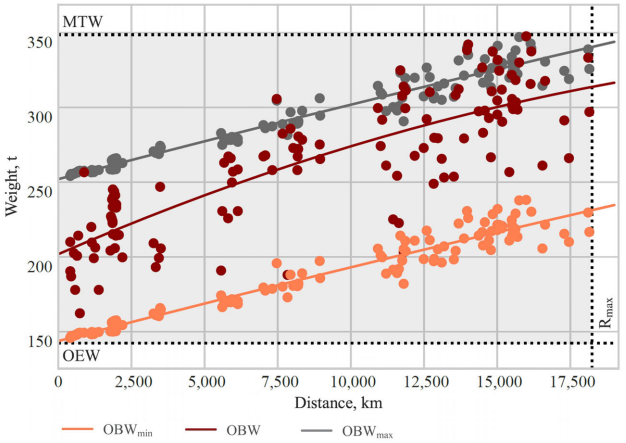

FIG 5. Overview of the weight assumptions derived from regression approaches (colored solid line) and the train DPs (colored points) as baseline for the calculation input data (own figure).

The authors used 137 FDR reports as the training baseline to aggregate the respective input OBW for the subsequent calculation. The reader should note that the limiting approaches for the minimum and maximum OBW correlate with the respective constant structural limit weights of the OEW and MTW. In essence, the authors decided to align these two weight inputs with the necessity to operate the planned missions. Consequently, $\mathrm{OBW_{min}}$ and $\mathrm{OBW_{max}}$ must increase with ground distance. The specific values also

TAB 1. Parametrization of the OBW regression functions.

	OBW_{min}	OBW	OBW_{max}
b_0	143.81	202.36	252.08
b_1	0.01	0.01	0.01
b_2	$-1.65 \cdot 10^{-8}$	$-1.28 \cdot 10^{-7}$	$-1.65 \cdot 10^{-8}$

rely on the train data that allows one to explore the FC per individual FDR FE. Subsequently, the observed functions are parallel.
The three approaches (OBW_{min}, OBW, and OBW_{max}) were created using quadratic regression approaches. Here, the OBW_{min} and OBW_{max} achieved a coefficient of determination[10], R^2, of 0.94. The estimated actual OBW shows a reduced R^2 of 0.67. That behavior can be traced down to the influence of the payload of the individual FE as part of the train data set. Even though unpractical to reflect the reality, henceforth the authors assume similar payloads for the subsequent calculation regardless of the trajectory operator.
The gathered FC results are the starting point for the *Emission Evaluation*. As illustrated in Fig. 3, the approach to calculate the primary emission constituents was derived from the literature and defines the constant constituent parameters for carbon dioxide, CO_2, water, H_2O, and sulfur dioxide, SO_2, which is assumed to incorporate other sulfur oxides S_xS_y [11]. The evaluation of the secondary emission constituents follows the work of DuBois and Paynter from Ref. [39] (with further discussion in [5]) with the application of [40]. Here, the emission of nitrogen oxide, NO_x, carbon monoxide, CO, and hydrocarbon, HC, is based on the thrust setting. From a simplified point of view, the former is increased where the latter two are decreased with increasing thrust.

3. CASE STUDY - THE DATA STRUCTURE

In this section, the cleaned-up FR24 data is presented and analyses with regard to the structure and distribution are commenced. The data covers the years 2019 and 2022. The former is introduced as reference year prior to the corresponding influences from COVID-19 (year 2020 with biasing spurs into the following year). The latter comprises the first year of the Russian campaign against the Ukraine as introduced in Sec. 1.1.

One can observe significant data gaps above land masses. The largest areal data outages can be identified in the joint of central Sahara and subtropical/tropical Africa, as well as the area of the Highland of Tibet to the northern borders of the country of Mongolia. In particular, the data show no submitted DPs at and around the Crimean Peninsula that is also part of the aggressive political tension between the focused countries.
To summarize the 57,183 usable files of the year 2019, the B77L-operated individual FEs cover distances from 106.36 km to 17,828.32 km [12] performed by 227 aircraft. In μ, the B77Ls travelled 5,455.12 km with a σ of 3,454.51 km. The major portion lies in the range of 2,648.43 km (Q1) to 7,376.20 km (Q3). In total, usable data from the global B77L fleet comprise 312,295,033.28 km of ground distance in 2019 (with reported 26,708,469 DPs).

The analysis has revealed that Qatar Airways commenced 9,441 FEs or a share of 16.51% of the present data set, followed by FedEx Express (15.77% $\widehat{=}$ 9,016 FEs). Further airline shares are depicted in Fig. 19 that offers to identify all operators with more than 2,000 FEs commenced in 2019[13]. Notably, the four major airlines of the Arabic peninsula (Qatar Airways, Emirates, Etihad Airways, Saudi Arabian Airlines, and Iraqi Airways) are responsible for 34.61% of all B77L FEs in 2019. In comparison, the total share is composed from

1) American operators (24.90%),
2) Asian airlines (18.38%),
3) European operators (14.66%), and
4) Others (7.43%).

The authors have also evaluated the FEs with regard to the shares in freighter and passenger service. In fact, the reader should note that this assessment cannot be evaluated exactly from the given data. A coarse B777 separation could be made with the data request for the ICAO aircraft code B77L[1]. It is noteworthy that multiple airlines use the B77L's passenger and freighter version equally, e.g., Qatar Airways, Emirates, or Ethiopian Airlines. Subsequently, by default, the state *passenger service* was assigned generalising, in an airline's mixed fleet (passenger and freighter service, both) the transport of goods on freighter aircraft are identified as subordinate. The identified shares can, therefore, be interpreted as an estimated minimum share for freighters, as only all-freighter airlines are identified correctly. Coherently, the portion of passenger airlines are prone to be interpreted as maximum assumption. However, with 52.88% is the minimum freighter share in B77L operation in 2019 is still higher than the passenger service share of 47.05%.

In 2022[13], the cleaned data set provided comprises 78,366 FEs performed by 281 aircraft. In fact, the flight movements are composed of 49,404,910 DPs that is a significant absolute increase of 84.98% in available scope of DPs. Here, the shortest FE with

[10] The use of the adjusted coefficient of determination, R^2_{adj}, is neglected as no additional descriptive variables were added.
[11] $EI_{CO_2} := 3{,}160\,g\,kg^{-1}$, $EI_{H_2O} := 1{,}230\,g\,kg^{-1}$, $EI_{SO_2} := 0.84\,g\,kg^{-1}$.
[12] Minimum ground distance: CDG/LFPG to ORY/LFPO performed by AF370Y, Maximum ground distance: SFO/KSFO to DEL/VIDP performed by AI174
[13] Henceforth, the term "year" is used for the time interval from 1st January to 31st August of the respective year.

141.32 km was performed on the 23rd August 2022[14]. The maximum distance travelled was DOH/OTBD to DFW/KDFW performed by QR731[15]. In general, in 2022 (compared to 2019) n_{FE} increased by 36.99% to 427,340,297.16 km.

Similarly to above's approach, Fig. 6 illustrate the 2-D distribution of DPs across the earth's surface and the corresponding data rate per grid field of 1°-1° resolution. Notably, the local concentration of DPs is exceptionally high in the Greater Hongkong area, now with an even more prominent DP density of 2.24% (of 2022's DPs) in the area of the UAE.

The data rate mean value μ is improved to 0.14 Hz with a standard deviation σ of 0.15 Hz. Additionally, 50% of the values (IQR) span 0.18 Hz around the arithmetic mean.

When analysing airline performance, it is clear that Qatar Airways again drives the UAE share among airlines, Fig. 20 reveals. With the UAE share in performed flights remains relatively constant (34.71%), the differences can be, especially, identified in the number of FE originated by European (significant increase) and American operators (reduction in share). Here the The exact shares are calculated as follows:

1) American operators (21.77%),
2) Asian airlines (15.12%),
3) European operators (20.95%), and
4) Others (5.67%).

For Qatar Airways Tab. 2 even unveils the significant increase in absolute *FE/day* of +29.17% within three years. Additionally, the authors highlight development of German cargo operators like Lufthansa Cargo and Lufthansa's joint venture (with DHL), Aerologic. With extensive growth, the former managed to add 165.48% to the FE commenced per day. Already being a stable B777F operator, Aerologic even added +15.71 flights per day to its schedule.

TAB 2. Flights performed per airline with more than 2,000 FEs per year as lists inner join.

Airline	2019	2022	ΔFE/day[16] , -	ΔFE/day[16], %
Qatar Airways	9,441	16,499	+29.17	+74.76
FedEx Express	9,016	11,024	+8.30	+22.27
Aerologic	4,588	8,389	+15.71	+82.85
Emirates	7,399	7,283	−0.48	−1.57
Korean Air	4,635	5,019	+1.59	+8.28
Ethiopian Airlines	4,247	4,442	+0.81	+4.59
Lufthansa Cargo	1,405	3,730	+9.61	+165.48
Turkish Airlines	1,631	3,229	+6.60	+97.98
EVA Air	2,222	3,170	+3.92	+42.66
Southern Air[17]	2,021	1,614	−1.68	−20.14

Compared to 2019, the number of B777 all-freighter FEs (as determined above) increased by 4.76%. In 2022 in total 45,172 FEs were performed by the B777's freighter version. In turn, in the first eight months of 2022 30,240 flights were commenced on a B777-200LR.

4. RESULTS

In this section we illustrate the fuel consumption and, thus, the emission composition of the FEs penetrating and bypassing the focal airspaces of the Russian-Ukraine conflict based on the model introduced in Sec. 2.3.

The established Reduction Procedure.

The proposed approach imposes a narrowing reduction to FEs with relevance, which, furthermore, will be clustered to ensure consistent analysis using multiple analysis focus frames as proposed in Fig. 8.

Here, Fig. 8 depicts that five steps were tested for validity and, subsequently, analyzed with regard to the key parameters (e.g., FC, Emissions). The initial reduction to the usable FEs can be traced back to the process introduced in Sec. 2.1 that is visualized in Fig. 2. As originally stated in the previous chapter, this step leaves 57,183 and 78,366 trajectories to be analyzed for 2019 and 2022. In further process tasks, the authors concentrate on a FN-focussed approach (3) that determines the role of FNs in an operators network with respect to the airspace restrictions. In (3a) the total FNs per complete airline set and per operator are focussed. The reader should note that this approach lacks of comparability as the data reference baseline is altered between the focal years. Thus, in (3b) the FNs are reduced to a relevant subset. This decision is based on the intransparent use of FNs, especially, in freighter operation as illustrated in Fig. 18. In this early stage, the reader should note the critical clustering into FNs to determine the aviation's environmental burden added by the airspace restrictions in Ukraine and Russia. The authors identified multiple operational change options (Apart from trajectory alteration) that are deduced when comparing a reference flight number FN_{Ref} of 2019 to the pendant in 2022: A) The 2022's FN is operated alike FN_{Ref}. B) Further stations are inserted to the original Origin/Destination (O/D) connection of FN_{Ref} as, e.g., refuelling of the aircraft is necessary to accomplish the planned reference mission. C) The mission of FN_{Ref} is appended with further stations before and/or after the reference mission. D) The FN is cancelled/unused/reassigned in 2022. E) In general, diversions are of relevance irrespective of the focussed year. Therefore, the FN-reduction in itself is valid, but arguably in terms of intercomparability betwenn 2019 and 2022 as the frame of reference is altered.

Nevertheless, observations found in (3a) and, subsequently, (3b) issued the establishment of relevant single O/D connections as well as the closing focus on individual routes operated per airline.

[14] CGN/EDDK to LGG/EBLG performed by FX9001

[15] Henceforth, the authors use the International Air Transport Association (IATA) and ICAO code as airport designator.

[16] Evaluated in the relevant time interval inter-annually between 2019 and 2022.

[17] Ceased operation and merged into Atlas Air, thus adapted in the evaluation.

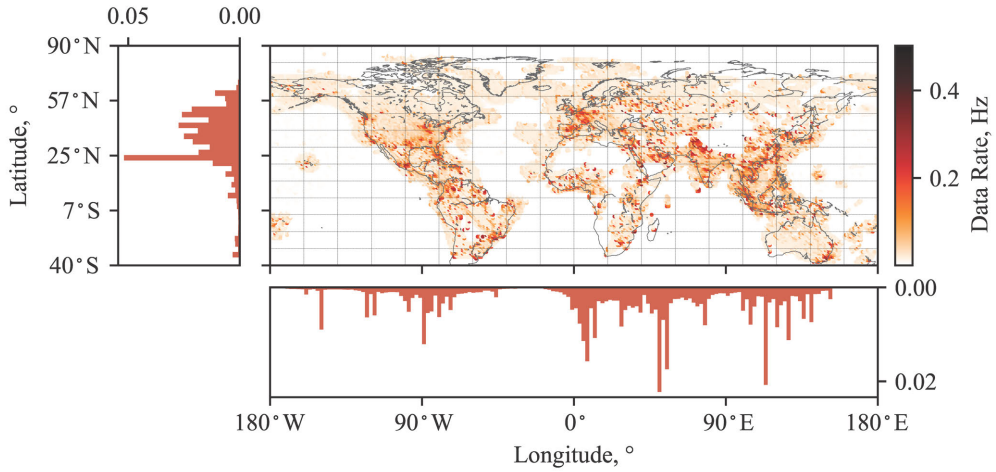

FIG 6. Global distribution of data rate and 2D-position of provided DPs of the year 2022 (own figure).

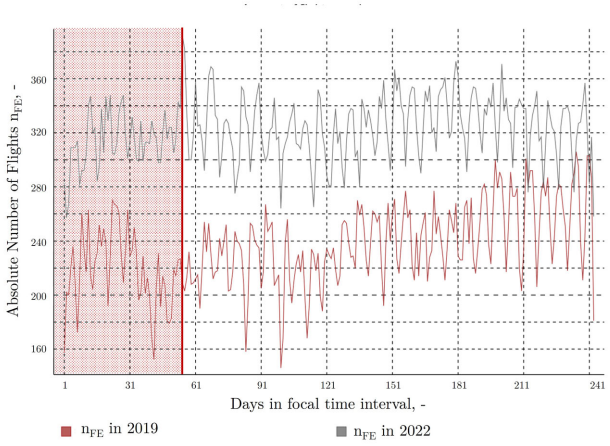

FIG 7. Daily B77L operation in n_{FE} as per submitted data set per time interval with the Russian invasion initiated on day 54 (own figure).

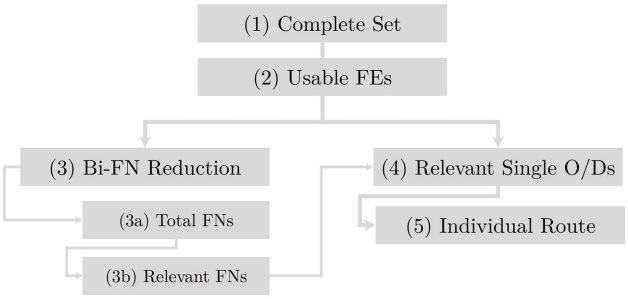

FIG 8. Applied reduction process to establish the relevant FEs (own figure).

Due to the unsatisfying results using the procedural step (3a) and (3b) in the present paper the results of the steps (4) and (5) are highlighted solely.
To further accomplish the reduction of FEs to the respective trajectories of relevance, the authors introduce the used focal airspaces of Ukraine and Russia that might be penetrated by aircraft operating specific routes.

The Airspace Definition.

In the light of FR24 data and to expose the penetrating flights, the authors implement a bi-criterial approach. Firstly, to identify the overflown countries, the minimum distance (great circle) to the next available airport per DP[18] was calculated based on the airport database provided through David Megginson's *OurAirports.com* that was further appended manually as this offers airports to be assigned to Ukraine and Russia. Taking into account Fig. 11, assumptions were introduced regarding the Russian mainland east of the Ural mountains with relevance to the regions of the Kamchatka Peninsula, Sakhalin, and Kuril Islands. In those areas, the demographic density is relatively low and, thus, can be characterised as remote, which imposes the necessity of heliports, small airfields next to small airports. Therefore, the iterative determination of the closest airport returns affected trajectories that seem to be located outside of Russian airspace. This effect also considers the open waters Easterly of Russia where similar problems were identified. In fact, the critical aerodromes here are, e.g., Petropavlovsk-Kamchatsky Airport, Iturup Airport, Yuzhno-Kurilsk Mendeleyevo Airport, Severo-Kurilsk Vertodrom, Nikolskoye Airport, Ust-Kamchatsky Airport, Yuzhno-Sakhalinsk Airport, Aeroport Preobrazheniye, Vladivostok International Airport, or Airport Lavrentiya as they are of a remote nature. Furthermore, this procedure is also limited when considering Southern bypasses of the airspace in the vicinity of the international airports of Sochi, Simferopol, Kosh-Agach, Nalchik, or Sevastopol. Finally, considering the Ukrainian airspace the west-

[18]The acquisition of the geolocations, independent of the open-access data source, understandably shows hard daily bulk request limits with one of the more generous limits using GeoPy's geocoders with temporal limiters.

ern borders are influenced by the proximity to the Uzhhorod and Chernivtsi International Airport.
Notably, the authors experienced similar behaviour with the comprehensively developed remote locations in the centre of Russia (in the area from the Ob river to the Lena river) where the assignment of the nearest-airport lead to significant great circle distances.

FIG 9. Clustering of sectors and location of critical remote aerodromes for the identification of the Ukrainain/Russian airspace (own figure).

Thus, the respective year's trajectories are analysed for the penetration of the highlighted airspaces shown in Fig. 9 created with [41]. In addition to the nearest-airport approach that is prone to impose uncertainty, e.g., above international waters, the authors introduce an underlying procedure to improve the identification of trajectories penetrating the Ukrainian and Russian airspaces. Hence, the respective airspaces are defined by polygonial structures created, e.g., per [41] (including Kaliningrad) as well as Ukraine's territory borders that are illustrated in Fig. 9.

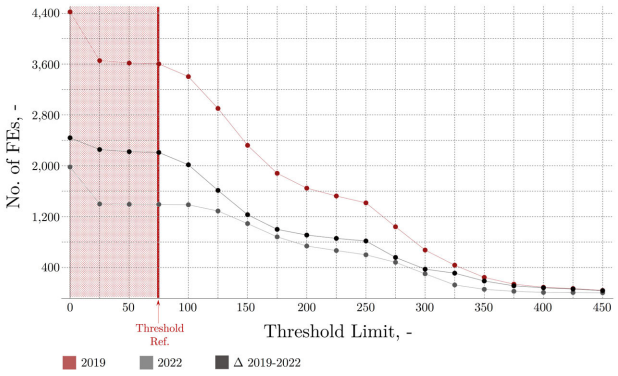

FIG 10. Influence of the threshold value with the accepted FEs (from usable files) above the Ukrainian and Russian airspace (own figure).

As FR24 data sets experience company-internal filtering, the authors determined to use a threshold value of 75 that rejects trajectories with the cumulated penetrating n_{DP} per FE less than the said value as irrelevant to the airspace penetration. The authors' experience shows that, e.g., airlines bypass the Ukrainian airspace with just minimal lateral distance for example in the area around Uzhhorod International Airport. Thus, the threshold value ensures consistent identification of relevant FEs.

Total Emissions of 2019 and 2022.

Initially, we highlight the FC and emissions created in the respective years regardless of airspace restrictions. The model estimates the total FC in the focal time interval of the reference year to 2,386,265.78 t consumed on 53,826 FEs (further rejection of 5.87% of the usable files). Here, only LH FEs are responsible for the consumption of 1,931,025.95 t of fuel ($\widehat{=}$ 80.92% of fuel used in the three clusters SH, MH, and LH). As a consequence, the total CO_2 emission amounts to 7,540,599.86 t. Furthermore, the authors want to highlight the 43,224.35 t of the total NO_x emitted in the airport vicinities.
As mentioned above, the model identified an increase in n_{FE} by 18,634 flights, still leaving the increase in usable FEs at 25.72%. The total calculated FC is 3,253,331.94 t of kerosene with an average FC of 44.90 t per individual FE (+0.57 t compared to 2019). The FC composition within the clusters changed in negligible magnitude. However, in 2022 an average of 77.00 FEs per day are added, increasing the CO_2 emission by 2,739,929.08 t (+11,322.02 t per day) and circa 1mio.t. of H_2O (+4,406.99 t per day). The air at and around the 260 used airports is altered, e.g., by 59,038.81 t of NO_x.

The Establishment of the Reference State in 2019.

When analysing the usable trajectories (2) for penetration of the established polygonal airspaces in the relevant time frame from 24th february to 31st August, the formed subset (3a) for the year 2019 is constructed of 3,603 FEs in 216 unique flight numbers performed by 17 B777 operators[19]. In this year, the Russian and Ukrainian airspace was used extensively by Korean Air on 778 ($\widehat{=}$ 21.59% of the FEs), followed by China Southern Airlines on 646 occasions. The German operators Aerologic and Lufthansa utilised the relevant airspaces on 668 FEs (320 and 348 FEs respectively), in majority, on their flights to/from Far East (e.g., Japan, China, or Singapore). Of the 3,603 flights, 2,710 FEs are performed by all-freighter B77L operators. Congruently to Chpt. 3, in a relative perspective, this translates to a minimum of 75.22% of the flights performed by these operators.
Compared to the results previously presented, the relevant flight events using at least one of both airspaces comprise 5.03% of the total usable FEs performed by a B77L. Therefore, the results reveal the natural operational change in subset characteristics that is induced by the geographic location and surface area of Russia and Ukraine. Hence, just 1.08% of the flight events crossing the Ukrainian and Russian airspace

[19]The reader should note that, e.g., Aerologic performs flights under Lufthansa Cargo's identifier.

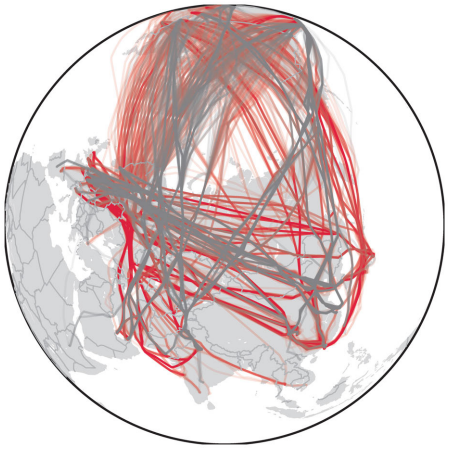

FIG 11. Relevant trajectories fulfilling the penetration criteria of the Russian and Ukrainian airspace per year (24th Feb to 31st Aug) (own figure).

are of a SH nature (below 180 min considering the μ of 168.01 $\pm$ 9.22 min). The composition in FEs above 180 min the majority of flights are longer than 360 min (94.17%).
From 24th February to the end of August 2019 the collective flights cumulatively used 286,142.16 t of kerosene. As reported in Tab. 3, this directly translates into the CO_2-emission of 904,209.23 t. When reducing this approach to the Ukranian and Russian airspace alone, for the year 2019 the authors estimate the emission of at least 301,916.58 t of CO_2 in the Russian airspace as source (assuming no dispersion of air parcels).
For the complete set of penetrating FEs, the proposed model estimates the possibly contrail-creating H_2O emission (acc. to [17] dependent on temperature and water vapour pressure assuming isobaric mixing) to at least 351,954.86 t with 117,518.16 t alone above both airspaces. The reader should note that the share of high-altitude 4-D positions of the B77L above the relevant airspaces is significant. Indeed, 65.06% of the submitted states are located at altitudes greater than or equal to 9 km. Taking into account the Ukrainian and Russian airspaces, 94.58% of the n_{DP} is located higher than or at 9 km. With the indirect height dependence in the contrail composition, this result introduces a substantial Global Warming Potential for the respective time period.

The Changes in the Focal Airspaces in 2022.

In the focus period from 24th February to 31st August 2022, the amount of relevant flight events was considerably reduced to 1,393 FEs due to the extensive inbound ban of Western operators as shown in Fig. 12 (grey trajectories). Individual FEs can be separated into 223 unique flight numbers performed by 18 airlines. The reader should note that the identified n_{FE} is depicted in Fig. 11 with no position submitted in Ukrainian airspace in 2022.

Unaffected by the inbound ban into Russia, Air India performed the most FEs penetrating this focus airspace on 318 occasions. The model ascertains further operators using the, generalizing, advantageous routes across Russia more than 100 times in 2022:

- Air China (295 FEs),
- Ethiopian Airlines (171 FEs),
- Pakistan International Airlines (135 FEs),
- Emirates (118 FEs), and
- China Southern Airlines (115 FEs).

In total, at least 44.15% of the trajectories were performed by all freighter operators (in terms of B77L).

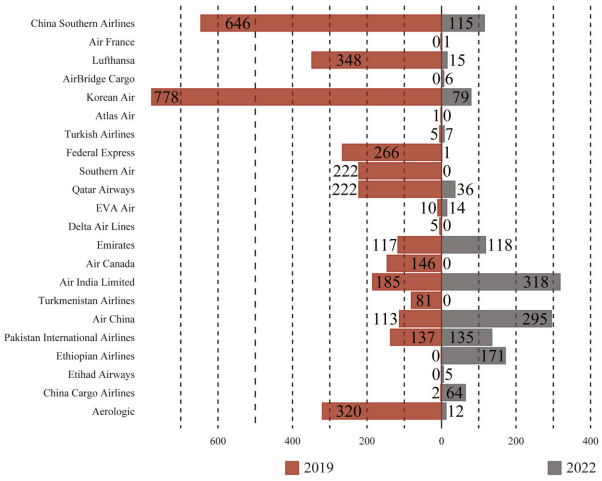

FIG 12. Comparison of the Airline Composition (fulfilling the criteria for relevant FEs) penetrating the Ukrainian and Russian Airspaces per year (24th Feb to 31st Aug) (own figure).

When focussing on the single flight events, the relative flight composition changed marginally. Additionally, an increased portion of FEs can be allocated to the LH section (98.35%). In total, the average flight time amounts to 771 min with 50% of the value between 623 min and 925 min. The maximum flight time sits at 1,126 min. No FE was shorter than or equal to 180 min.
Naturally, only 38.92% of fuel was consumed in 2022, compared to the year 2019. Here, the cumulative FC amounts to 111,371 t that translates to 352,147 t of CO_2 and 137,070 t of H_2O, the authors report with Tab. 3. Respectively, the share of primary constituents emitted in Russian airspace is 23.29%. Due to the FE composition with the majority of FEs of a flyover nature, the total amount of NO_x estimated to be emitted as low as 2,019.42 t. When reducing the frame of consideration from the complete trajectory to the Russian airspace only, 622.24 t of NO_x was emitted. In fact, due to the significant amount of LH FEs just 1.13% can be allocated to the narrow atmospheric band below 1 km where in this band itself 63.00% of the portion are emitted in the ground-near zone up to 0.10 km.
The complete frame reduction is considered adequate as no trajectory penetrated Ukrainian airspace, as the country is in a state of war coinciding with further

Level 3 risk evaluation (assuming the categorisation of the DFS). The consequential mass-wise emission evaluation can be aggregated from Tab. 3.

The Changes outside of the Focal Airspaces in 2022.

Due to the inbound prohibition/ban into both airspaces, it can be concluded that the respective flight movements extensively circumvent the area to fulfill the flight to a destination. Consequently, the initial task lies in the deduction of relevant FEs allowing an acceptable comparison considering the increased complexity. The increase is a consequence of the comprehensive area to be avoided. That infers further constraints into the aircraft operation, especially in the MH and LH portion.

Following the above listed items A) to E), the analysis infers more complexity when striving to identify the changes, and, thus, the environmental burden added to the transport system outside of the relevant airspaces. To understand this behaviour, the authors identified the connections used per FN in the reference year. Only 14 of the 586 unique flight numbers are operated between a single unique O/D connection (see element (4) of Fig. 8). The maximum O/D assignment is identified for *FX21*. The operator assigned the FN to 27 different O/D connections (see Fig. 18).

To narrow down the paper focus, the author choose to highlight the identification of critical individual single O/D routes.

When analysing single routes operated by Aerologic, the authors identified the route from Hongkong (HKG/VHHH) to Leipzig (LEJ/EDDP) as the most critical route that was performed 179 times. In that direction, the model calculates an additional average FC of 9.43 t (from 87.11 t per FE in 2019). The IQR of the FC distribution's results is broadened to 4.61 t. However, return connections to Hongkong experience an average FC per FE increase of 5.95 t ($\widehat{=}$ 7.90%) with the IQR rising by 72.37%. The σ increases by 29.04% in the year 2022. The average flight time increased by 59.64 min with an extra distance of 743.17 km. The most critical routes are summarised in Tab. 4 together with the respective emissions in Tab. 11.

Similarly to Fig. 13, although routes to India (Bangalore and New Delhi) penetrated the airspaces of interest in 2019, a slight reduction in FC per FE in 2022 was identified, identifying their influence on the network's FC as marginal.

The second German operator with importance to the present paper is Lufthansa Cargo. The airline alone is the source of an average increase of 28.39 t of CO_2 per FE ($\widehat{=}$ 11.22%), consistent with the increase in FC. Notably, the FC's σ increased from 4.54 t to considerable 10.41 t. The FC distribution's $\tilde{m}$ even increased by 11.10 t. In total, the German operator emitted 60,213.48 t of CO_2. Approximately 39.87% of the carbon dioxide's mass is added by the emission of H_2O.

FIG 13. The trajectories of the German airlines Aerologic and Lufthansa Cargo operating a single O/D pair in 2019 (red) and 2022 (black distribution) (own figure).

Furthermore, the authors identified the most critical routes of Lufthansa Cargo. When highlighting the average parameters of flight time and FC, the critical route is operated from Seoul Incheon to Frankfurt. In a year-to-year comparison, the increase in both parameters lies well above 20% resulting in an added time cost to 835.60 min increasing the FC to 99.17 t. However, the average ground distance travelled of the route from Frankfurt to Tokio-Narita describes this parameter's maximum impact.

The authors identified a further operator with relevance to the topic but with a substantial need for adjustment. With their main hub Seoul, Korean Air operated to European airports (i.e., Vienna Schwechat, Milano Malpensa, London Heathrow, Frankfurt Airport, Paris Charles de Gaulle, Stockholm/Arlanda and Oslo Gardermoen). Adversely, the hub's beneficial location with respect to North America routes to New York JFK, Vancouver International Airport, Los Angeles, or Anchorage are part of the data set submitted. Both areas include FEs in 2019 that penetrated the focal airspaces. The provided trajectories are shown in Fig. 14.

Nevertheless, certain Korean Air flight numbers were identified to cross the relevant airspaces (under the condition introduced by Fig. 9) in 2019 and 2022. Especially for the latter year, their relevance is negligible. Exemplary, the authors want to highlight the flight number *KE273* that was used multiply on different O/D connections. The proposed procedure identified the direct flights from Seoul to Anchorage and Seoul to Miami as relevant to the analysis. Unfortunately, the flight number was also used to connect Miami and Anchorage in 2022 plus further connecting flights from Miami to South America (São Paulo-Congonhas/Brazil, Campinas International Airport/Brazil, and La Nubia Airport in Manizales/Columbia) were operated under the FN. As these flights are partially short and do not reflect this paper's focus, further manual rejection was performed on ten other flight numbers.

Hence, the authors identified 717 cumulative Korean Air FEs (2019: 385; 2022: 332) as ready to be statis-

TAB 3. Overview of substances emitted in total and in the Ukrainian and Russian airspaces assessed through the proposed model in the time interval from 24th Feb-31st Aug in the years of 2019 and 2022.

Frame	Year	Mass of Primary Constituent m, t			Mass of Secondary Constituent m, t		
		CO_2	H_2O	SO_2	NO_x	CO	HC
Total	2019	904,209.23	351,954.86	240.36	5,255.71	1,096.00	63.15
	2022	352,146.86	137,069.82	93.61	2,019.42	408.01	22.00
Above UKR/RUS	2019	301,916.58	117,518.16	80.26	1,653.10	287.89	9.77
	2022	115,157.71	44,824.05	30.61	622.24	105.48	3.26

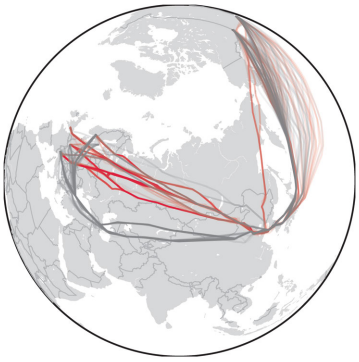

FIG 14. The trajectories of Korean Air operating various O/D pairs in 2019 (red) and 2022 (black distribution) after a manual FN rejection process (own figure).

tically assessed. The evaluation of fuel consumption reveals significant changes for the B77L operator from Korea: in 2019 the average FC on the reduced FEs was 70.16 t with σ of 15.86 t. When avoiding Russian airspace, Korean Air on average has to consume an additional 11.36 t of kerosene per FE to commence its routes (with similar σ). This increase in average FC pushes the results distribution's median in equal orders of magnitude while reducing the IQR slightly by 2.03 t in FC per FE. Korean Air's average flight time increased by 49.49 min to 703.02 min on additional 996.08 km (2019: 8,876.78 km).

The airline's CO_2 emission per FE (in μ) increased by 22.96% to 48.11 t. In a total view on the year 2022, Korean Air emitted 82,946.52 t of CO_2 and 32,286.15 t of H_2O. The total NO_x emission could be reduced by 1.21% to 481.40 t.

As Korean Air is a prohibition/ban affected airline, the authors managed to deduce the most critical connection commenced by the airline based on the provided data. Generally, this pertains the operators routes to Europe. Regardless of the average parameters presented in Tab. 4, the relative highest cost is imposed to operate from Stockholm-Arlanda to Seoul Incheon when compared to 2019. The efforts rose above 30% with the FC even increased by +39.30%. Coherently presented by Tab. 11, the amount of primary constituents emitted relates evenly and amounts to an 276.94 t of CO_2 and 107.80 t of H_2O emitted on average per FE on the route. Compared to 2019, NO_x increased by +45.33 altering air in the vicinty of airports.

As introduced above, the FN issue is even more stringent with FedEx Express' B77L operation. Identified FNs in 2019 are not uniquely used on the routes in both focal years. Therefore, an empirically correct comparative view to other B77L operators is questionable as a common baseline is missing. A similar approach as in the FN reduction of Korean Air flights was chosen. Hence, just 130 FEs were of importance to the topic (reduced from 175 FEs; 2019: 88 FEs, 2022: 42 FEs) that are visualised in Fig. 15.

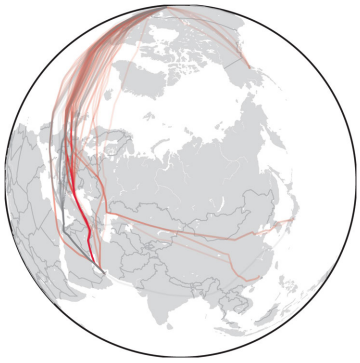

FIG 15. The trajectories of FedEx Express operating various O/D pairs in 2019 (red) and 2022 (black distribution) after a manual FN rejection process (own figure).

As a consequence of above's finding, together with the flight time and ground distance, the FC per FE and, thus, the corresponding emission evaluation showed no significant change. Therefore, further analysis is neglected, e.g., on an individual route basis. The founding results with regard to the reference establishment can be aggregated from Tab. 5 in coherence with Tab. 6. Additional comparison offer Tab. 7 with Tab. 8.

As expected, next to the above-mentioned negative effects on operators when comparing both years, the results also indicate that there are winners of the crisis. Naturally, these are the operators unaffected by the restrictions. In general, all identified unaffected operators, except for China Southern Airlines[20], increased

[20] According to the proposed model's FN analysis, the airline reduced to operate to London Heathrow or Amsterdam Schiphol in 2022 and experienced cut-backs on their connections to the United States of America (Los Angeles, Anchorage) that pre-

their nuumber of rotations and even added new connections to their network with B77L network growth rates up to 2,000% (Air China added 38 rotations to their 2 rotation network from 2019).
Exemplary, the authors want to highlight the results aggregated through an unaffected Air India's operation.

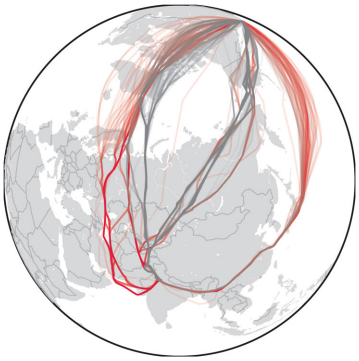

FIG 16. The trajectories of Air India operating various O/D pairs in 2019 (red) and 2022 (black distribution) (own figure).

With the trajectories illustrated in Fig. 16, Air India even achieved a significant reduction in FC per FE (corresponding to the reduced flight time and distance travelled). In comparison to other unaffected operators, the airline achieved lower growth rates (in terms of the B77L network) with 123.51%[21]. Here, the difference can be deduced from the (identified by the model) in 2019 already high number of commenced FEs of 251. The Fig. 16 introduces the reason for the savings in FC per FE. As identifiable by the provided red lateral positions, Air India managed to circumvent the Southern departure routes around Pakistan, Afghanistan in the western direction, and the Himalayas on the eastern routes. That is also deductable to India's conflict with Pakistan as well as the political instabilities in Afghanistan.
In turn, this allows the airline to reduce the average fuel burn per FE by 19.14 t (the relative σ increased by 9.58% in the frame of consideration). The network's $\tilde{m}$ was significantly reduced by 30.57%. As a consequence of the airline's rerouting option, an average of 60.48 t of CO_2 was not emitted per FE compared to 2019. Even in the statistical maximum, 31.20 t of Greenhouse Gas were saved, thus reducing Air India's environmental burden in the considered time frame (similarly related is the reduction in H_2O and SO_2). With regard to secondary emission constituents, the average NO_x emission per FE was reduced greatly by 0.37 t (to 1.54 t). However, the effect is statistically minimised by an increase of the IQR by 11.72% (see exact values in Chpt. 7). In total, 476.13 t of NO_x was emitted.

viously penetrated the Russian airspace. The growth rate was -358.49%.

[21] Cf. Qatar Airways: 1,050.00%, China Cargo Airlines: 155.00%, Pakistan International Airlines: 184.62%.

Further notable results can be deduced from the operation of Pakistan International Airlines. This is an operator allowed to use Russian airspace. Based on the identified network as visualised in Fig. 17 and assuming Russian ATC does not prefer specific operators, PIA avoided Turkmenistan in the year 2022. It can be assumed that Russia offers just a few entry points into the airspace when arriving from the South such that fixed areas in the northern portion of Kazakhstan must be approached (year 2022). On four occasions PIA even circumvents the Ukrainian airspace on a Westerly route increasing the result's IQR. The maximum distance travelled was operated in 2019 where PIA's operation 2022 suffers from a significant broadening of the ground distance by 492.68 km. Nevertheless, PIA experienced a slight improvement of the FC per FE from 98.01 $\pm$ 6.35 t to 96.71 $\pm$ 6.96 t. On the other hand site, the maximum FC calculated experienced an increase of 1.88% to 114.99 t. Naturally, this leads to a slight decrease in primary constituents and the emitted NO_x. The other two focal secondary emission constituents (CO and HC) increased in the frame of consideration.

FIG 17. The trajectories of Pakistan International Airlines operating various O/D pairs in 2019 (red) and 2022 (black distribution) (own figure).

On a global level, the authors showed that there are beneficiaries and disadvantaged operators of the focal airspace restriction. Mostly, these clusters are built with respect to the operator's country of origin's relation to Russia (the airspace penetration prohibition in Ukraine can be considered a concern of all civil B77L operators). Korean Air can be identified as part of the latter group. Furthermore, from the presented findings in coherence with Tab. 9 and Tab. 10 that on dedicated routes/FNs the German operators cannot ensure optimal trajectory planning requiring a minimum amount of fuel consumed. Compared to the complete set of relevant airlines (in terms of the proposed model), Aerologic and Lufthansa Cargo "suffer" from the airspace prohibition and ban in Ukraine and Russia on an above-average level. This can clearly be derived using Tab. 9 when compared to the total results. Here, it shows the significant decrease in total flight time by (−7.89%) that results in a considerable added total FC of −11.58%. That translates to an overall

+8.50% increased total FC considering the entire set of airlines.
The effect is even harsher when one compares the German operator with the conglomerate of the other 8 airlines. When compensating for that, the Δ_{rel} in FC rises to 12.34% in added fuel consumption compared to the non-German operators. The relation reflects on the emission of primary and secondary constituents whose year-to-year (2019-2022) difference is notable. Besides the other significant increases in emissions, the authors want to highlight the rise in NO_x per FE that amounts to an added 1.64% of emission for Aerologic and Lufthansa Cargo. To further ensure comparability, the reader should note that the respective total results underlie an increase in aircraft movements per FN. Thus, intercomparability is recommended.

5. DISCUSSION & OUTLOOK

Following the composition of the extensive data provided by FR24, the authors presented a method to identify the influence of the bypass of the Ukrainian and Russian airspace as a consequence of the Russian agitation against Ukraine inititated on 24th February 2022 to aviation and operators of different regions. To account for the operational differences imposed by COVID-19 in the years 2020 and 2021, the year 2019 is identified as the appropriate reference. Earlier years would introduce an even more significant uncertainty due to the already rapid changes in, e.g., network routes or operator fleets. In the focal time intervals in 2019 and 2022 data was provided for the time period from 1st January to 31st August, respectively. In total, 51,604 and 69,062 FEs were considered usable for further analysis.
The proposed results are highly dependable on the FR24 data input. This also implies limitations for a consistent evaluation across years. The authors assume that the input reference changed over the years as, e.g., the composition of the company's receiver network as well as the data quality improved. For two FEs (one per focal year) this might impose an increased data rate, because the sensor network density in a certain area increased when comparing 2019 to 2022. This development is supported with the company's extrinsic motivation to extend the network with own or FR24-built receivers. In addition to the presumed alteration in the data aggregation setup, the data composition itself is described by an increase in aircraft movements from 21,183 ($\widehat{=}$ 37.04%), among other things, imposed by an increase in the B77L-fleet of 55 units.
As part of the proposed methods, a range of analyses were performed. Initially, the total FC results and the corresponding emissions in both years are provided. The authors' findings revealed the composition in B777 operations in terms of SH, MH, and LH flights. Naturally, the LH portion represents the main FE type responsible for the FC. Here, a total of 1,827,309.69 t of kerosene were consumed. This amounts to an emission share of 55.32% where the SH flights describe the lowest share portion. Notably, the global amount in average FC per FE increased marginally from 44.23 t in the reference year to 44.82 t in the time period in 2022. Subsequently, the increase in total FC of 813,273.84 t can be traced back to the increase in aircraft movements using B77L. Based on this initial and general approach, the authors introduced an analysis of FNs that penetrated the airspaces of interest. Consequently, the airspace polygons were roughly defined as visualised in Fig. 9. Although a border- and source-based airspace definition approach was followed, the authors account for discrepancies or imprecise definition with a total penetration threshold of 75 DPs in the polygons per FE that is accompanied by a second nearest-airport criteria. The combined assessment, a valid evaluation to airspace penetration was made. Nevertheless, the underlying second approach could be adjusted, e.g., for a geolocation request per position submitted though this increases computational costs significantly when using open-source data. Additionally, such an approach might also include incorrect country identifications, especially above high waters. Furthermore, one might vary the defined threshold value to determine to investigate the accompanying change in operator composition entering the focal airspaces.
As follows, the identified single FEs operating in Ukrainian or Russian airspace were clustered according to the FN used on the connection. The authors consider the results of the subsequent analysis as unsatisfying. Clearly, a reduction in focal aircraft movements is considerable, but still included trajectories irrelevant to the present paper's topic. It was experienced that, other than passenger connections, many freighter operators use a flight number on different, even unrelated, routes. Based on the data submitted, the authors identified FedEx Express to use an unique FN on 30 different routes (including unrelated and connecting routes) operated by B77L - assuming the input data set as single-source-of-truth. The relation was proven in both focal time periods and, thus, imposes uncertainty to the statistical evaluation. Therefore, it is assumed that due to the airspace prohibition/ban especially freighter operators reacted more flexible on the restrictions with added destinations in to previously directly operated routes. It can be assumed that these additional stops cannot be solely traced back to refueling stops. The authors claim that the freighter operators network can be adjusted with additional payload added at added stations to reduce total economic pressure and incorporated losses. The broadly determined relation is prone to a high share in freighter operators using B77L.
Additionally, the authors identified FNs in 2022 where the original 2019 route was initiated from an inserted origin airport, following the 2019 route and with further connection to another final destination. Inserted or appended stations (to the reference route) might also vary, which raises difficulties of FN and route referencing.

TAB 4. Summary of most critical Routes per affected Airline evaluated in the Average Performance Parameters per FE.

Airline	Route (IATA-/ICAO-code)	Ground Distance, km	Flight time, min	FC, t
Aerologic	HKG/VHHH - LEJ/EDDP	10,102.46 (+7.94%)	747.81 (+8.67%)	96.54 (+10.82%)
	LEJ/EDDP - HKG/VHHH	10,165.69 (+8.59%)	670.66 (+6.70%)	81.32 (+7.90%)
Lufthansa Cargo	ICN/RKSI - FRA/EDDF	10,112.91 (+12.66%)	835.60 (+24.62%)	99.17 (+21.95%)
	FRA/EDDF - NRT/RJAA	11,622.59 (+18.73%)	773.84 (+13.56%)	92.40 (+17.07%)
	FRA/EDDF - PEK/ZBAA	9,217.07 (+15.29%)	623.90 (+7.81%)	71.95 (+11.72%)
Korean Air	CDG/LFPG - ICN/RKSI	10,453.94 (+11.26%)	783.64 (+20.86%)	88.07 (+16.09%)
	FRA/EDDF - ICN/RKSI	10,162.96 (+12.78%)	683.95 (+9.68%)	83.56 (+13.98%)
	OSL/ENGM - ICN/RKSI	10,461.42 (+27.92%)	697.98 (+24.45%)	87.13 (+30.54%)
	ARN/ESSA - ICN/RKSI	10,688.01 (+36.10%)	716.50 (+30.96%)	87.64 (+39.30%)

In a last step, the connection network analysis per FN was used to determine the used routes as innerjoin across the time period. As a consequence of the overlaying increase in aircraft movements, it was shown that the analysis per FN-based route per operator offers comparability. Here, the authors assumed that certain FNs are operated by just one operator such that, i.e., Lufthansa Cargo operates the identified FNs solely.

Subsequently, the trajectories of the affected operators and those of operators unaffected by the prohibition/ban were analysed. For the year-wise comparison, the authors want to present an actual picture of the consumed kerosene and emissions, and therefore assumed a similarly strong influence of the weather. Applying the introduced model in coherence with the proposed selection (and rejection) method on the provided data operated by B77L only, the authors identified multiple critical routes of Korean Air to experience the most significant increase in FC of up +39.30% on their route from Stockholm to Seoul (ARN/ESSA - ICNRKSI) when being banned from using the Russian airspace. Additionally, the route from Oslo to Seoul (OSL/ENGM - ICN/RKSI) describes another connection with circa a 30.00% increase in FC. Lufthansa Cargo's Seoul Incheon connection was identified as the most critical route for a German operator (third critical on a global view). Underlying the present weather and the connections offered further analysis can be commenced per operator network where the operators effort added can be combined with the present weather and possible routes creating an individual effort/demand matrix per operator.

In a further analysis aiming for trajectory comparability, the input weather data might be fixed to determine the added effort to commence certain missions. Notably, that approach can only be used with ban-affected airlines if the routing uncertainty is assumed to be similar. The authors also want to highlight that the presented results are based on an already validated model that imposes uncertainty. For example, the model underestimates μ by −3.72% with a σ of 11.98% when being exposed to FR24 data. This fact must be taken into account when judging the validity of the results for further extensive analyses. The authors recommend the proposed assessment described in Sec. 2.3 with Fig. 5 where an input weight corridor is established between OBW_{min} and OBW_{max}. As the presented results are based on the determined validation-based OBW, the evaluation of the corridor might introduce additional insights. That approach would also broaden the results possible in the corridor of variation in input OBW as the FC and payload weight will vary among the various operators. Hence, an emission spread is created.

To further broaden the corridor, the parameter OBW_{max} is highlighted. Here, with a recursive calculation approach with reference to the landing with the structural limitation Maximum Landing Weight can be insightful. In this approach, it should be assumed that the aircraft's on-block is performed with no usable fuel remaining but maximum payload possible transported.

Additionally, the authors want to highlight the analysis opportunities imposed when future researchers might get access to an airline's payload mass additionally. Hence, network adjustments would be detectable

according to external factors and further predictions of global network changes might be performed. This can greatly elaborate the estimation of aviation-based future environmental burden extensively.
Lastly, as an enhancement in scope, the authors plan to use the data baseline of FR24 on the calculation of other sources of emission as the main engine's oil consumption and the Auxiliary Power Unit's FC. Such an extension is assumed to improve the holistic view on operational aircraft emissions.

6. ACKNOWLEDGMENT

The authors express gratitude to an undisclosed operator. Without its expertise this study would not have been realizable. Furthermore, we want to gratefully thank the company FlightRadar24 for the provision of the trajectories. We also want to thank Felix Jacques Langermann for his effort for parts of the introductory portion.

Contact address:

eric.schuster@tu-berlin.com

References

[1] D. Poles. *Base of Aircraft Data (BADA) Aircraft Performance Modelling Report.* EUROCONTROL Agency; EUROCONTROL Experimental Centre, Centre de Bois des Bordes; B.P.15; F – 91222 Brétigny-sur-Orge CEDEX; FRANCE, eec technical/scientific report no. 2009-009 edition, Mar. 2009. [retrieved 07 Apr 2020].

[2] K. Seymour, M. Held, G. Georges, and K. Boulouchos. Fuel estimation in air transportation: Modeling global fuel consumption for commercial aviation. *Transportation Research Part D: Transport and Environment*, 88:1–16, nov 2020. ISSN: 1361-9209. Paper 102528, [retrieved 08 Jan 2021]. DOI: 10.1016/j.trd.2020.102528.

[3] D.K. Wasiuk, M.H. Lowenberg, and D.E. Shallcross. An aircraft performance model implementation for the estimation of global and regional commercial aviation fuel burn and emissions. *Transportation Research Part D: Transport and Environment*, 35:142 – 159, mar 2015. ISSN: 1361-9209. [retrieved 23 Jul 2020]. DOI: 10.1016/j.trd.2014.11.022.

[4] Yashovardhan Sushil Chati and Hamsa Balakrishnan. A gaussian process regression approach to model aircraft engine fuel flow rate. In *2017 ACM/IEEE 8th International Conference on Cyber-Physical Systems (ICCPS)*, pages 131–140, 2017. [retrieved 17 Feb 2021]. DOI: 10.1145/3055004.3055025.

[5] Donald J. Sutkus, Steven L. Baughcum, and Douglas P. DuBois. Scheduled civil aircraft emission inventories for 1999: Database development and analysis. Technical report, Boeing Commercial Airplane Group, P.O. Box 3707 Seattle, Washington 98124, Oct. 2001. Final Contractor Report NASA CR 2001-211216, [retrieved 08 Jun 2020].

[6] ICAO. *ICAO Carbon Emissions Calculator Methodology.* ICAO, 10 edition, June 2017. Version 10, [retrieved 23 Apr 2021].

[7] Brandon Graver, Kevin Zhang, and Dan Rutherford. Co2 emissions from commercial aviation, 2018. Technical report, International Council on Clean Transportation (ICCT), 1500 K Street NW, Suite 650, Washington, DC 20005, 9 2019. Working Paper 2019-16, [retrieved 17 Jun 2020].

[8] Junzi Sun and Irene Dedoussi. Evaluation of aviation emissions and environmental costs in europe using OpenSky and OpenAP. In *The 9th OpenSky Symposium.* MDPI, dec 2021. [retrieved 23 Jul 2022]. DOI: 10.3390/engproc2021013005.

[9] Eric Schuster and Maarten Uijt de Haag. Multimodel integration for fuel-related aircraft emission estimation on boeing 777. *Journal of Aerospace Information Systems*, pages 1–13, jun 2022. DOI: 10.2514/1.i011042.

[10] Volker Grewe. Climate impact of aviation: Co2 and non-co2 effects, and examples for mitigation options. Technical report, Deutsches Zentrum für Luft- und Raumfahrt (DLR), Institute for Atmospheric Physics, 01 2018. [retrieved 13 Sep 2020].

[11] U. Schumann, H. Schlager, F. Arnold, R. Baumann, P. Haschberger, and O. Klemm. Dilution of aircraft exhaust plumes at cruise altitudes. *Atmospheric Environment*, 32(18):3097 – 3103, 1998. ISSN: 1352-2310. [retrieved 12 Jul 2020]. DOI: 10.1016/S1352-2310(97)00455-X.

[12] U. Schumann. On the effect of emissions from aircraft engines on the state of the atmosphere. *Annales Geophysicae*, 14:365–384, 1994. [retrieved 24 Jun 2020]. DOI: 10.1007/s00585-994-0365-0.

[13] P. Forster, V. Ramaswamy, P. Artaxo, T. Berntsen, R. Bett, D.W. Fahey, J. Haywood, J. Lean, D.C. Lowe, G. Myhre, J. Nganga, R. Prinn, G. Raga, M. Schulz, and R. Van Dorland. *Changes in Atmospheric Constituents and in Radiative Forcing*, chapter 2, page 204. Cambridge University Press, Cambridge, United Kingdom and New York, NY, USA, 2007. [retrieved 18 Jun 2020].

[14] Mauro Masiol and Roy M. Harrison. Aircraft engine exhaust emissions and other airport-related contributions to ambient air pollution: A review. *Atmospheric Environment*, 95:409 – 455, Oct. 2014. ISSN: 1352-2310. [retrieved 18 Jun 2020]. DOI: 10.1016/j.atmosenv.2014.05.070.

[15] D.S. Lee, G. Pitari, V. Grewe, K. Gierens, J.E. Penner, A. Petzold, M.J. Prather, U. Schumann, A. Bais, T. Berntsen, D. Iachetti, L.L. Lim, and R. Sausen. Transport impacts on atmosphere and climate: Aviation. *Atmospheric Environment*, 44(37):4678 – 4734, 2010. ISSN: 1352-2310. Transport Impacts on Atmosphere and Climate: The ATTICA Assessment Report, [retrieved 09 Jul 2020]. DOI: 10.1016/j.atmosenv.2009.06.005.

[16] Changlie Wey and Chi-Ming Lee. *Aircraft emissions: gaseous and particulate*, chapter 2, page 23. CRC Press, 1 edition, 9 2017. [retrieved 18 Jun 2020]. DOI: 10.1201/b20287-2.

[17] Klaus M. Gierens. *Contrails and Contrail Cirrus*, chapter eae352, pages 1–11. American Cancer Society, 10 2010. ISBN: 9780470686652. [retrieved 09 Jun 2020]. DOI: 10.1002/9780470686652.eae352.

[18] Marcus O. Köhler. *Global Atmospheric Chemistry and Impacts from Aviation*, chapter eae347, pages 1–10. American Cancer Society, 2015. ISBN: 9780470686652. [retrieved 08 Jun 2020]. DOI: 10.1002/9780470686652.eae347.pub2.

[19] K. Dahlmann, V. Grewe, S. Matthes, and H. Yamashita. Climate assessment of single flights: Deduction of route specific equivalent co2 emissions. *International Journal of Sustainable Transportation*, 0(0):1–12, 2021. [retrieved 02 Aug 2023]. DOI: 10.1080/15568318.2021.1979136.

[20] DFS Deutsche Flugsicherung GmbH. Aic 12/23 flugverbote und flugbetriebliche empfehlungen zu krisengebieten durch das bundesministerium für digitales und verkehr (bmdv) - luftfahrthandbuch deutschland (aip germany). Online, July 2023. [retrieved 07 August 2023]. https://aip.dfs.de/BasicIFR/2023JUL13/chapter/e53aae0f42de75b5aab8d56086c768aa.html.

[21] FAA Federal Aviation Administration. Kicz notam a0004/22 — security — united states of america prohibition against certain flights in the lviv (uklv), kyiv (ukbv), dnipro (ukdv), simferopol (ukfv), and odesa (ukov) flight information regions (fir), as well as, the kyiv upper information region (uir) (ukbu). Online, Feb. 2022. [retrieved 07 August 2023]. https://www.faa.gov/air_traffic/publications/media/KICZ_A0004-22_Prohibitory_NOTAM-Ukraine_all_FIRs_and_UIR_(2022024_1930Z).pdf.

[22] FAA Federal Aviation Administration. Kicz notam a0005/22 — security — united states of america prohibition against certain flights in the specified areas of the moscow (uuwv), samara (uwww) and rostov-na donu (urrv) flight information regions (fir). Online, Feb. 2022. [retrieved 07 August 2023]. https://www.faa.gov/air_traffic/publications/media/KICZ_A0005-22_Prohibitory_NOTAM-Russia_MOSCOW_SAMARA_and_ROSTOV_FIRs_(20220224_1930Z).pdf.

[23] Xiaoyong Wang, Jun Zhang, and Sebastian Wandelt. On the ramifications of airspace bans in aero-political conflicts: Towards a country importance ranking. *Transport Policy*, 137:1–13, Apr. 2023. ISSN: 0967-070X. [retrieved 07 Aug 2023]. DOI: https://doi.org/10.1016/j.tranpol.2023.04.003.

[24] Chairussani Abbas Sopamena. The global impact of russian aerospace closure. *Jurnal Dinamika Global*, 7(01):161–177, jun 2022. ISSN: 2548-9216. [retrieved 07 Aug 2023]. DOI: 10.36859/jdg.v7i01.984.

[25] Peterson K Ozili. Global economic consequence of russian invasion of ukraine. *SSRN Electronic Journal*, Feb. 2022. [retrieved 07 Aug 2023]. DOI: 10.2139/ssrn.4064770.

[26] Araz Akbarli, Ezgi Begüm ÖndeŞ, Dilek Gezer, and Birsen Açikel. The impact of the ukraine-russia conflict on the aviation sector: February-may 2022. *Journal of Aviation*, 6(3):346–354, nov 2022. DOI: 10.30518/jav.1125560.

[27] Satria Unggul Wicaksana Prakasa, Asri Wijayanti, Achmad Hariri, and Levina Yustitianingtyas. The effect of russia–ukraine war on international aviation sectors. *KnE Social Sciences*, oct 2022. [retrieved 07 Aug 2023]. DOI: 10.18502/kss.v7i15.12132.

[28] Organisation for Economic Co-operation and Development and International Transport Forum. How the war in ukraine impacts aviation – and whatto do about it. *Transport Policy Responses to the War in Ukraine*, (3), Dec. 2022. [retrieved 07 Aug 2023].

[29] Aya Tanikawa. Flight routes and map projections. Online, Mar. 2022. [retrieved 07 Aug 2023]. https://blog.datawrapper.de/flight-routes-map-projections/.

[30] IATA Internation Air Transport Association. Iata factsheet - the impact of the war in ukraine on the aviation industry. Online, Mar. 2022. [retrieved 07 August 2023]. https://www.iata.org/en/iata-repository/publications/economic-reports/the-impact-of-the-conflict-between-russia-and-ukraine-on-aviation/.

[31] A. V. Sokolov. Titanium metal markets and the russian aviation industry. *Problems of Economic Transition*, 54(3):65–78, 2011. [retrieved 07 Aug 2023]. DOI: 10.2753/PET1061-1991540305.

[32] David Yu and Tasos Michael. The ukrainian conflict: Impact on the aviation finance and leasing industry. *The Journal of Structured Finance*, 28(2):33–41, jul 2022. [retrieved 07 Aug 2023]. DOI: 10.3905/jsf.2022.1.141.

[33] RTCA, Inc. Minimum aviation system performance standards for automatic dependent surveillance - broadcast (ads-b) change 1. techreport RTCA DO-242B, RTCA, Inc., 1828 L Street, NW, Suite 805, Washington, DC 20036-5133, USA, Dec. 2006. [retrieved 04 Aug 2023].

[34] RTCA, Inc. Minimum operational performance standards for universal access transceiver (uat) automatic dependent surveillance - broadcast (ads-b). techreport RTCA DO-282B, RTCA, Inc., 1828 L Street, NW, Suite 805, Washington, DC 20036-5133, USA, Dec. 2009. [retrieved 04 Aug 2023].

[35] RTCA, Inc. Minimum operational performance standards for 1090 mhz extended squitter automatic dependent surveillance - broadcast (ads-b) and traffic information services - broadcast (tis-b). techreport RTCA DO-260B, RTCA, Inc., 1828 L Street, NW, Suite 805, Washington, DC 20036-5133, USA, Dec. 2009. [retrieved 04 Aug 2023].

[36] Junzi Sun. *The 1090 Megahertz Riddle: A Guide to Decoding Mode S and ADS-B Signals*. TU Delft OPEN Publishing, 2 edition, 2021. ISBN: 978-94-6366-402-8. [retrieved 02 Oct 2021]. DOI: 10.34641/mg.11.

[37] Martin Strohmeier, Vincent Lenders, and Ivan Martinovic. Security of ads-b: State of the art and beyond. *IEEE Communications Surveys & Tutorials*, 17, 07 2013. [retrieved 04 Aug 2023]. DOI: 10.1109/COMST.2014.2365951.

[38] Flightradar24 AB. How flight tracking works, 2023. [retrieved 04 Aug 2023]. https://www.flightradar24.com/how-it-works.

[39] Doug DuBois and Gerald Paynter. "fuel flow method2" for estimating aircraft emissions. *SAE Technical Paper*, page 16, 08 2006. ISSN: 0148-7191. [retrieved 19 Nov 2020]. DOI: 10.4271/2006-01-1987.

[40] ICAO. *Introduction to the ICAO Engine Emissions Databank*. International Civil Aviation Organization, 1995. [retrieved 02 Jun 2020].

[41] State Air Traffic Management Corporation of the Russian Federation. Atc centre structure. Online, 2023. [retrieved 16 Jul 2023]. https://gkovd.ru/en/joint-atm-system/atc-centres-structure/.

7. APPENDIX

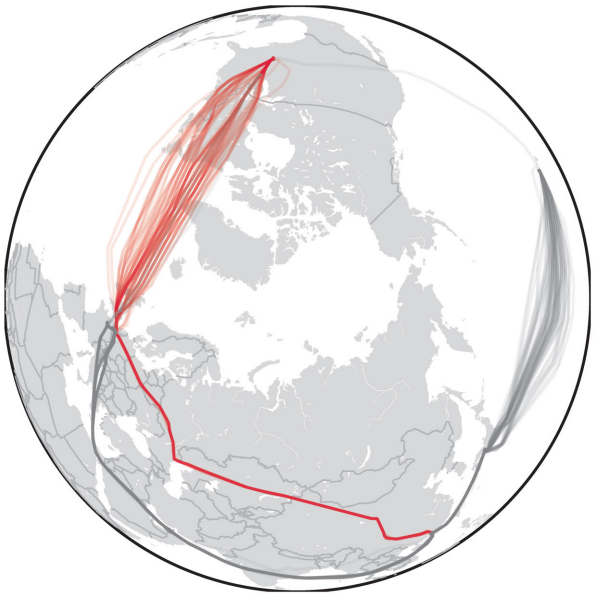

FIG 18. FN-reduced trajectories of FedEx Express FX21 operating among 27 destinations (own figure).

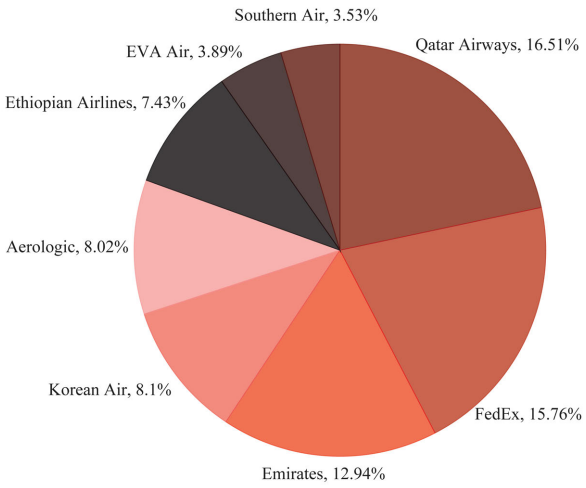

FIG 19. Shares of airlines with more than 2,000 FEs in 2019 (own figure).

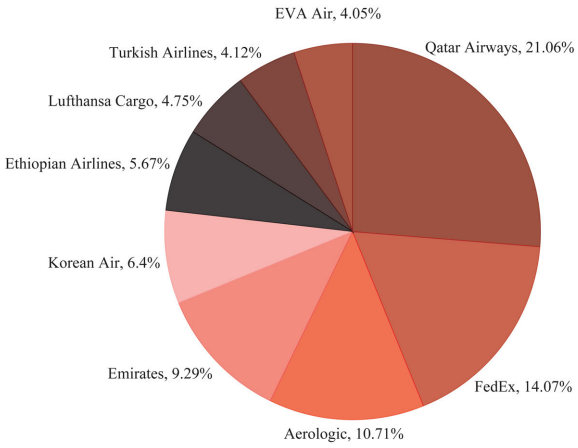

FIG 20. Shares of airlines with more than 2,000 FEs in 2022 (own figure).

TAB 5. Performance Analysis per Airline of relevant Parameters after a manual FN Rejection Process in the Reference Year 2019.

Airline (IATA-/ICAO-code)	Affected by airspace restrictions	Number of FEs, -	Performance parameters per FE (μ - σ - IQR)		
			Ground Distance, km	Flight time, min	FC, t
Aerologic (3S/BOX)	X	336 (425)	7,296.14 || 2,382.47 || 1,895.53	540.10 || 153.74 || 147.29	66.29 || 22.92 || 20.13
Air India (AI/AIC)		251 (251)	14,963.04 ||913.80 || 1,884.75	1,009.81 || 72.14 || 120.42	104.10 || 20.46 || 41.24
Air China (CA/CAA)		2 (15)	8,200.24 || 122.66 ||122.66	572.62 || 4.88 || 4.88	64.35 || 3.23 || 3.23
China Cargo Airlines (CK/CKK)		20 (27)	1,757.86 || 1,704.51 || 53.46	148.12 || 106.25 || 12.80	14.12 || 14.08 || 1.59
China Southern Airlines (CZ/CSN)		570 (710)	8,004.25 || 3,420.07|| 5,815.43	569.90 || 233.83 || 404.02	62.89 || 27.43 || 54.07
FedEx Express (FX/FDX)	X	88 (116)	12,352.83 || 1,842.93 || 141.90	860.01 || 96.62 || 71.04	97.42 || 13.70 || 12.59
Korean Air (KE/KAL)	X	385 (516)	8,876.78 || 946.52 || 720.44	653.53 || 70.11 || 86.05	70.16 || 15.86 || 13.81
Lufthansa Cargo (LH/GEC)	X	318 (428)	9,368.78 || 430.18 || 816.58	675.40 || 22.89 || 28.20	80.06 || 4.54 || 5.88
Pakistan International Airlines (PK/PIA)		78 (108)	11,844.46 || 617.16 || 346.57	822.41 || 39.69 || 41.34	98.02 || 6.35 || 9.51
Qatar Airways (QR/QTR)		2 (2)	4,975.09 || 87.11 || 87.11	383.41 || 4.76 || 4.76	40.30 || 1.02 || 1.02
Total		2,050 (2,598)	9,384.83 || 3,312.11 || 1,664.05	668.72 || 214.97 || 163.73	74.85 || 25.55 || 22.11

TAB 6. Emission Analysis per Airline of relevant Parameters after a manual FN Rejection Process in the Reference Year 2019.

Airline (IATA-/ICAO-code)	Affected by airspace restrictions	Mass of Primary Constituents per FE, t (μ - σ - IQR)		Mass of Secondary Constituents per FE, t (μ - σ - IQR)	
		CO_2	H_2O	NOx	CO
Aerologic (3S/BOX)	X	209,491.59 || 72,442.68 || 63,611.44	81,542.61 || 28,197.62 || 24,760.15	1,261.94 || 466.56 || 361.68	266.00 || 59.76 || 60.88
Air India (AI/AIC)		328,948.54 || 64,648.07 || 130,313.52	128,040.10 || 25,163.65 || 50,723.30	1,910.73 || 310.87 || 547.83	376.73 || 106.87 || 212.70
Air China (CA/CAA)		203,346.72 || 10,195.88 || 10,195.88	79,150.78 || 3,968.65 || 3,968.65	1,221.41 || 9.71 || 9.71	226.46 || 49.58 || 49.58
China Cargo Airlines (CK/CKK)		44,606.38 || 44,507.35 || 5,021.95	17,362.61 || 17,324.06 || 1,954.75	242.42 || 270.90 || 58.60	127.57 || 46.12 || 44.60
China Southern Airlines (CZ/CSN)		198,746.44 || 86,693.47 || 170,853.52	77,360.16 || 33,744.61 || 66,503.11	1,182.11 || 529.40 || 1,080.75	230.12 || 77.77 || 129.66
FedEx Express (FX/FDX)	X	307,844.60 || 43,303.40 || 39,798.90	119,825.59 || 16,855.44 || 15,491.34	1,749.25 || 319.54 || 311.88	437.40 || 134.27 || 221.54
Korean Air (KE/KAL)	X	221,699.28 || 50,107.99 || 43,655.32	86,294.34 || 19,504.06 || 16,992.42	1,265.71 || 286.63 || 294.98	271.35 || 72.06 || 59.70
Lufthansa Cargo (LH/GEC)	X	252,982.56 || 14,344.54 || 18,566.10	98,471.06 || 5,583.48 || 7,226.68	1,439.69 || 115.35 || 152.80	309.25 || 30.54 || 26.33
Pakistan International Airlines (PK/PIA)		309,738.52 || 20,074.32 || 30,058.76	120,562.78 || 7,813.74 || 11,700.09	1,784.62 || 158.20 || 241.07	340.77 || 32.18 || 21.70
Qatar Airways (QR/QTR)		127,359.68 || 3,220.78 || 3,220.78	49,573.55 || 1,253.66 || 1,253.66	696.26 || 23.85 || 23.85	203.14 || 0.82 || 0.82
Total		236,510.67 || 80,749.51 || 69,860.53	92,059.53 || 31,430.98 || 27,192.55	1,377.73 || 474.16 || 457.32	286.05 || 95.08 || 78.34

TAB 7. Performance Analysis per Airline of relevant Parameters after a manual FN Rejection Process according to the Restrictions in Ukrainian and Russian Airspace in 2022.

Airline (IATA-/ICAO-code)	Affected by airspace restrictions	Number of FEs, -	Performance parameters per FE (μ - σ - IQR)		
			Ground Distance, km	Flight time, min	FC, t
Aerologic (3S/BOX)	X	349 (416)	7,524.25 || 2,936.59 || 6,934.97	546.53 || 191.99 || 440.15	66.34 || 27.07 || 57.32
Air India (AI/AIC)		310 (338)	13,491.43 || 417.39 || 443.74	943.76 || 41.61 || 38.58	84.96 || 22.42 || 39.14
Air China (CA/CAA)		40 (63)	8,276.38 || 366.44 || 140.35	573.85 || 24.51 || 22.96	67.82 || 6.14 || 5.46
China Cargo Airlines (CK/CKK)		31 (41)	4,662.56 || 3,890.55 || 7,866.93	341.08 || 237.95 || 488.20	40.52 || 32.45 || 64.37
China Southern Airlines (CZ/CSN)		151 (194)	4,479.95 || 1,596.17 || 99.95	330.88 || 108.32 || 21.52	36.94 || 11.34 || 2.30
FedEx Express (FX/FDX)	X	42 (59)	12,778.33 || 1,724.58 || 78.49	834.91 || 101.34 || 33.55	97.79 || 12.92 || 5.51
Korean Air (KE/KAL)	X	322 (449)	9,872.86 || 789.63 || 1,230.68	703.02 || 61.22 || 66.82	81.52 || 13.30 || 11.78
Lufthansa Cargo (LH/GEC)	X	214 (321)	11,103.09 || 991.05 || 137.58	749.53 || 70.34 || 38.81	89.04 || 10.41 || 10.41
Pakistan International Airlines (PK/PIA)		144 (196)	11,716.83 || 465.71 || 839.24	825.71 || 49.28 || 56.45	96.71 || 6.96 || 10.01
Qatar Airways (QR/QTR)		21 (35)	1,633.72 || 1,152.43 || 59.40	136.89 || 83.72 || 10.57	12.15 || 9.60 || 2.05
Total		1624 (2112)	9,710.55 || 3,364.75 || 3,368.98	683.59 || 224.39 || 252.27	75.51 || 26.07 || 29.54

TAB 8. Emission Analysis per Airline of relevant Parameters after a manual FN Rejection Process according to the Restrictions in Ukrainian and Russian Airspace in 2022.

Airline (IATA-/ICAO-code)	Affected by airspace restrictions	Mass of Primary Constituents m per FE, t (μ - σ - IQR)		Mass of Secondary Constituents m per FE, t (μ - σ - IQR)	
		CO_2	H_2O	NOx	CO
Aerologic (3S/BOX)	X	209,629.39 || 85,528.23 || 181,130.33	81,596.25 || 33,291.05 || 70,503.26	1,252.22 || 541.69 || 1,100.84	259.86 || 72.82 || 132.42
Air India (AI/AIC)		268,463.66 || 70,842.17 || 123,696.16	104,496.93 || 27,574.64 || 48,147.56	1,535.90 || 371.57 || 612.02	317.64 || 112.08 || 197.46
Air China (CA/CAA)		214,300.99 || 19,413.24 || 17,252.92	83,414.63 || 7,556.42 || 6,715.54	1,231.05 || 124.93 || 127.23	252.14 || 42.44 || 32.07
China Cargo Airlines (CK/CKK)		128,054.53 || 102,538.42 || 203,410.95	49,844.01 || 39,912.11 || 79,175.78	741.67 || 600.09 || 1,166.57	184.02 || 91.10 || 165.93
China Southern Airlines (CZ/CSN)		116,737.13 || 35,840.37 || 7,269.62	45,438.82 || 13,950.52 || 2,829.63	658.59 || 209.04 || 56.29	175.00 || 37.27 || 24.81
FedEx Express (FX/FDX)	X	309,014.55 || 40,830.28 || 17,413.50	120,280.98 || 15,892.80 || 6,778.04	1,775.36 || 261.87 || 153.32	361.18 || 59.55 || 31.88
Korean Air (KE/KAL)	X	257,597.89 || 42,015.24 || 37,234.42	100,267.53 || 16,354.03 || 14,493.15	1,495.02 || 250.50 || 261.95	310.89 || 76.32 || 33.91
Lufthansa Cargo (LH/GEC)	X	281,371.39 || 32,882.92 || 32,884.39	109,521.14 || 12,799.37 || 12,799.94	1,630.16 || 218.74 || 245.37	359.02 || 68.88 || 39.87
Pakistan International Airlines (PK/PIA)		305,616.96 || 22,003.95 || 31,619.75	118,958.50 || 8,564.83 || 12,307.69	1,733.52 || 163.34 || 195.80	351.45 || 57.62 || 29.98
Qatar Airways (QR/QTR)		38,384.60 || 30,342.93 || 6,469.71	14,940.84 || 11,810.70 || 2,518.27	214.78 || 172.04 || 56.42	113.21 || 42.57 || 44.71
Total		238,612.66 || 82,380.56 || 93,345.24	92,877.71 || 32,065.85 || 36,333.75	1,381.64 || 482.09 || 531.12	293.39 || 97.22 || 126.61

TAB 9. Summary of Performance Parameters per FE, cumulated for German Operators, and total cumulation.

		Ground Distance, km (Δ_{rel} to 2019)	Flight time, min (Δ_{rel} to 2019)	FC, t (Δ_{rel} to 2019)
Per FE	μ	9,710.55 (+3.47%)	683.59 (+2.22%)	75.51 (+0.89%)
	σ	3,364.75 (+1.59%)	224.39 (+4.38%)	26.07 (+2.02%)
	IQR	3,368.98 (+102.46%)	252.27 (+54.08%)	29.54 (+33.62%)
German Operators	Σ	5,002,024.21 (−7.89%)	351,139.85 (−11.39%)	42,207.00 (−11.58%)
Total	Σ	15,760,223.46 (−18.08%)	1,109,464.73 (−19.07%)	122,628.78 (−20.08%)

TAB 10. Summary of Performance and Emission Parameters per FE, cumulated for German Operators, and total cumulation.

		Mass of Primary Constituents per FE, t			Mass of Secondary Constituents per FE, t		
		CO_2 (Δ_{rel} to 2019)	H_2O (Δ_{rel} to 2019)	SO_2 (Δ_{rel} to 2019)	NO_x (Δ_{rel} to 2019)	CO (Δ_{rel} to 2019)	HC (Δ_{rel} to 2019)
Per FE	μ	238.61 (+0.89%)	92.88 (+0.89%)	0.06 (+0.89%)	1.38 (+0.28%)	0.29 (+2.57%)	0.02 (+2.93%)
	σ	82.38 (+2.02%)	32.07 (+2.02%)	0.02 (+2.02%)	0.48 (+1.67%)	0.10 (+2.25%)	0.01 (+9.39%)
	IQR	93.35 (+33.62%)	36.33 (+33.62%)	0.02 (+33.62%)	0.53 (+16.14%)	0.13 (+61.61%)	0.01 (+26.92%)
German Operators	Σ	133,374.13 (−11.58%)	51,914.62 (−11.58%)	35.45 (−11.58%)	785.88 (−10.88%)	167.52 (−10.76%)	10.14 (−9.90%)
Total	Σ	387,506.96 (−20.08%)	150,833.40 (−20.08%)	103.01 (−20.08%)	2,243.79 (−20.56%)	476.47 (−18.75%)	27.46 (−18.46%)

TAB 11. Summary of most critical Routes per affected Airline evaluated in the Average Emission Parameters per FE.

		Mass of Primary Constituents per FE, t			Mass of Secondary Constituents per FE, t		
Airline	Route (IATA-/ICAO-code)	CO_2	H_2O	SO_2	NO_x	CO	HC
Aerologic	HKG/VHHH - LEJ/EDDP	305.07	118.75	0.08	1.88 (+12.64%)	0.33 (+4.76%)	0.02 (+1.18%)
	LEJ/EDDP - HKG/VHHH	256.97	100.02	0.07	1.52 (+9.92%)	0.30 (+2.50%)	0.02 (−0.57%)
Lufthansa Cargo	ICN/RKSI - FRA/EDDF	313.39	121.99	0.08	1.84 (+23.34%)	0.46 (+53.76%)	0.03 (+96.28%)
	FRA/EDDF - ICN/RKSI	261.96	101.97	0.07	1.55 (+9.60%)	0.31 (+7.99%)	0.02 (+26.17%)
	FRA/EDDF - NRT/RJAA	291.97	113.65	0.08	1.69 (+21.24%)	0.36 (+10.76%)	0.02 (+7.78%)
	FRA/EDDF - PEK/ZBAA	227.35	88.49	0.06	1.32 (+17.58%)	0.33 (+28.06%)	0.02 (+44.43%)
Korean Air	CDG/LFPG - ICN/RKSI	278.30	108.32	0.07	1.55 (+15.35%)	0.48 (+59.15%)	0.04 (+108.98%)
	FRA/EDDF - ICN/RKSI	264.06	102.78	0.07	1.54 (+17.97%)	0.31 (+7.42%)	0.02 (+4.67%)
	OSL/ENGM - ICN/RKSI	275.32	107.17	0.07	1.62 (+36.97%)	0.32 (+20.69%)	0.02 (+13.68%)
	ARN/ESSA - ICN/RKSI	276.94	107.80	0.07	1.61 (+45.33%)	0.32 (+25.27%)	0.02 (+15.53%)